Landslides, bedrock incision and human-induced environmental changes in an extremely rapidly formed tropical river gorge

Toussaint Mugaruka Bibentyo [a,b,c,*], Antoine Dille [a], Arthur Depicker [d], Benoît Smets [a,e], Matthias Vanmaercke [d], Charles Nzolang [c], Stijn Dewaele [b], Olivier Dewitte [a]

[a] Department of Earth Sciences, Royal Museum for Central Africa, Tervuren, Belgium
[b] Department of Geology, Ghent University, Ghent, Belgium
[c] Department of Geology, Université Officielle de Bukavu, Bukavu, DR Congo
[d] Department of Earth and Environmental Sciences, KU Leuven, Leuven, Belgium
[e] Department of Geography, Vrije Universiteit Brussel, Brussels, Belgium

ARTICLE INFO

ABSTRACT

Landslides are hillslope processes controlled by natural changing topographic conditions. Landslides are also influenced by human activities. Yet, understanding the space-time occurrence of landslides and their interactions with these typically long-term natural and short-term human-induced controls remains a key challenge in many regions, especially in tropical environments where data scarcity is commonplace. Here we decipher these dynamic processes in the Ruzizi Gorge located in the Kivu Rift (Central Africa), that is an exceptional geomorphological landmark whose origin is associated with the rerouting of >7000 km^2 of drainage area from Lake Kivu during the Holocene. This bedrock river has also seen its landscape disturbed over the past decades by the development of the city of Bukavu (DR Congo). In this study, we combine detailed field observations, historical aerial photographs, archive analysis and satellite imagery to compile a multi-temporal inventory of 385 landslides and constrain their dynamics. We show that extremely high incision rates during the early stage of the formation of the gorge explain the space-time clustering of thousand-year-old large (up to ~2 km^2) landslides, independently from the lithological context. These landslides are currently non-active and poorly eroded. Their deposit areas partly cover the riverbed with boulders, armouring the channel and inhibiting further incision. The landslides that occurred over the last 60 years are shallower slope failures of smaller size and higher mobility. They tend to disappear rather quickly from the landscape, sometimes within a few years. Their distribution is primarily controlled by threshold slopes, lithology, and the past large landslides, the influence of the land use being less pronounced. Overall, the sediment mobilization rates associated with these high frequency landslides significantly outpace the extreme landslide erosion pulse associated with the gorge formation. Our results provide insight on interactions between channel-hillslope coupling and feedbacks among landslide processes and river gorge formation in a unique environment.

1. Introduction

Landslide processes are influenced by topographic steepening associated with bedrock river incision. In some places, e.g., the Himalaya, clusters of large landslides are observed along rivers with extremely rapid incision rates (e.g., 12 mm year^{-1} over periods of thousands of years; Burbank et al., 1996; Larsen and Montgomery, 2012). Causes to such river incision are numerous, including regional tectonic uplift (Burbank et al., 1996), as well as local changes in topography due to

river capture or an increase in discharge (Fan et al., 2018). Local changes can also come from infrequent flood events caused by the sudden release of large amounts of ponded water, which can lead to rates of erosion of several meters in a few days (Agatova et al., 2020; Baynes et al., 2015; Gupta et al., 2007; Lamb and Fonstad, 2010). Depending on the process at play, the rates of bedrock river incision can therefore vary dramatically. Since they are rare, landslide processes in extremely rapid river incision contexts remain yet poorly studied and understood (Burbank et al., 1996; Larsen and Montgomery, 2012; Yenes

---

et al., 2015). Bedrock river incision is further influenced by the lithology, including its strength and degree of weathering (Anton et al., 2015; Baynes et al., 2015; Campforts et al., 2020; Schanz and Montgomery, 2016; Whipple et al., 2022), which are factors that will as well modulate the mechanisms, their size, volume, and rates of occurrence of landslides (Clarke and Burbank, 2010; Dille et al., 2019; Henriques et al., 2015; Roda-Boluda et al., 2018).

The conversion of natural lands into human-dominated landscapes has dramatically accelerated over the past decades and is expected to continue in the future (Lambin et al., 2006; Lewis and Maslin, 2015). Drivers for this conversion include, among others, rapid – often informal – urban and agricultural expansion and associated deforestation (Cooper et al., 2018; Defries et al., 2010). These human-induced environmental changes are known to create conditions that favour slope instabilities, which leads to changes in landslide frequency, size, and mobilization rates (Bozzolan et al., 2020; Depicker et al., 2021a; Dille et al., 2022; Guns and Vanacker, 2014; Maki Mateso et al., 2023; Sidle and Ochiai, 2006).

While the role of river incision, lithology and human-induced processes on the occurrence and dynamics of landslides have been relatively well studied independently, reliable analyses of all these processes potentially acting in interactions are few (Broothaerts et al., 2012; Depicker et al., 2021a; Williams et al., 2021; Yenes et al., 2015). Here, we explore these interactions by focusing on the changing environment of the Ruzizi Gorge, a river gorge formed due to the exceptional rerouting of a large drainage system during the Holocene (Felton et al., 2007; Ross et al., 2014). The Ruzizi Gorge lies in a tropical mountainous region, an environment which remains largely under-researched in terms of landslide processes (Broeckx et al., 2018; Dewitte et al., 2022; Reichenbach et al., 2018). The gorge is formed into contrasting lithologies and includes both rural and urban landscapes. Within this study, we aim to (1) compile a detailed multi-temporal landslide inventory and identify the most sensitive areas to slope instabilities; (2) characterize these processes in relation to a reliable assessment of the coupling between bedrock channel incision and lithological characteristics; and (3) unravel the interactions between the natural and human-induced landscape changes in causing these slope instabilities. We focus on understanding the dynamics of the gorge based on detailed and reliable field-based observations supported by remote sensing.

2. The Ruzizi Gorge in the Kivu rift

Compared to the other Great Lakes of the East African Rift, Lake Kivu is relatively young. It formed during the late Pleistocene, when lavas from the Virunga Volcanic Province dammed the upper part of the Rift basin, which was at the time draining north towards the Nile River system (Fig. 1; Haberyan and Hecky, 1987; Ross et al., 2014). Alongside this damming, the level of the lake rose, reaching a maximum ~100 m above today's level at ~10 ka BP, when it started draining Kivu Rift waters (drainage area of 7380 km^2) southwards to Lake Tanganyika (Felton et al., 2007; Haberyan and Hecky, 1987; Ross et al., 2014; Stoffers and Hecky, 1978). The overflow took place at an overtopping location in Bukavu, developing into a gorge along a pre-existing fault system and resulting into the formation of the upstream reach of the Ruzizi River (Figs. 1 and 2). This incision process created a rejuvenated landscape in the pre-existing hydrographic network. Our study area includes this rejuvenated landscape and the relict landscape downslope the ridge crests closest to the gorge boundary (Fig. 1). In addition, the formation of the gorge is associated with the formation of a sediment deposit area of ~70 km^2 at its outlet. This deposit area contains an alluvial fan (partly eroded) and abandoned riverbeds (Ilunga, 1984, 2007; Ilunga and Alexandre, 1982; Fig. 1). The preserved alluvial fan is situated in the area now occupied by the town of Kamanyola. The Ruzizi Gorge represents a major geomorphological element in a region known to be intensely affected by landslides (Dewitte et al., 2021). However, our knowledge on the dynamics of formation and evolution of the Ruzizi

Gorge and the associated landslides remains limited.

Metasedimentary rocks and volcanic rocks form the two main lithologies of the Ruzizi Gorge. The metasedimentary rocks are of Mesoproterozoic age and consist of mica schists, quartzites and sandstones of the Bugarama group (Fernandez-Alonso et al., 2012; Villeneuve, 1977; Villeneuve and Chorowicz, 2004). These rocks show a relatively low degree of chemical weathering but are highly fractured. The volcanic rocks are of Miocene to Pleistocene age and belong to the South Kivu Volcanic Province (Fig. 1; Kampunzu et al., 1983; Kanika et al., 1981). They mainly consist of layers of basalt that is commonly intensively weathered, with regolith thicknesses that can reach several dozens of metres.

The Ruzizi Gorge experiences a tropical savanna climate (Peel et al., 2007), with a wet season from September to May and a dry season from June to August. Most of the recent landslides reported in the last two decades in the Kivu Rift region are rainfall-triggered and occur during the wet season (Monsieurs et al., 2018). These landslides are usually small and shallow features (Dewitte et al., 2021). The mobilization rates associated with the occurrence of new shallow landslides are increased over a period of typically 10 to 15 years after deforestation (Depicker et al., 2021b). Many of these small landslides tend to disappear from the landscape after a few years due to the rapid vegetation regrowth and agricultural practises in the region (Kubwimana et al., 2021; Maki Mateso et al., 2023).

Despite the important seasonality in the rainfall distribution, the discharge of the Ruzizi River at the outlet of Lake Kivu remains relatively constant throughout the year due to the overall high evapotranspiration in the region (Muvundja et al., 2014). Over the 1941–2015 period, the average discharge was 112 m^3 s^{-1}; while the maximum recorded discharge was 143 m^3 s^{-1} (Muvundja et al., 2022).

The diversity of agricultural landscapes and the presence of regional hydroelectric plants in the gorge are linked to the development of the city of Bukavu and its rapid population growth. The latter, particularly high since 1990, is in large part associated with political instability and chronic in*security* in the region that favoured migration towards the city and its surroundings (Michellier, 2017). Typically informal, the rapid growth of the city greatly contributed to the urbanisation of landslide-prone slopes (Dille et al., 2022).

3. Material and methods

3.1. Multitemporal landslide inventory

Depicker et al. (2020) compiled a regional landslide inventory covering our study area. This dataset was however created as a historical (geomorphological) inventory, i.e., reflecting the total number of landslide over time, and constructed over a much larger area. As a result, its construction involved the analysis of a limited number of satellite images at a very high spatial resolution (<1 m) from Google Earth available during 2000–2018 in a relative superficial way. Further, this inventory contains little information in terms of landslide process differentiation and does not include field-based observations. In our research we significantly improved this inventory by using various additional sources of information and more detailed process characterization (Table 1).

For each landslide, we determined the type, depth (shallow or deep-seated), relative age, year of occurrence, activity period and dimensions. The landslide type was defined according to the Varnes classification, updated by Hungr et al. (2014). Knowing that weathering and regolith formation can develop over important depths in the tropics, we defined a landslide as shallow when the depth of the main scarp was <5 m (following a similar methodology as Dewitte et al., 2021). When the height of the main scarp was >5 m, the associated movement was considered as deep. Large, deep-seated landslides have a morphology that can persist for thousands of years (Booth et al., 2017; Keaton and DeGraff, 1996). Following the approach proposed by Cardinali et al. (2002) and adapted by Dewitte et al. (2021), we assessed the relative
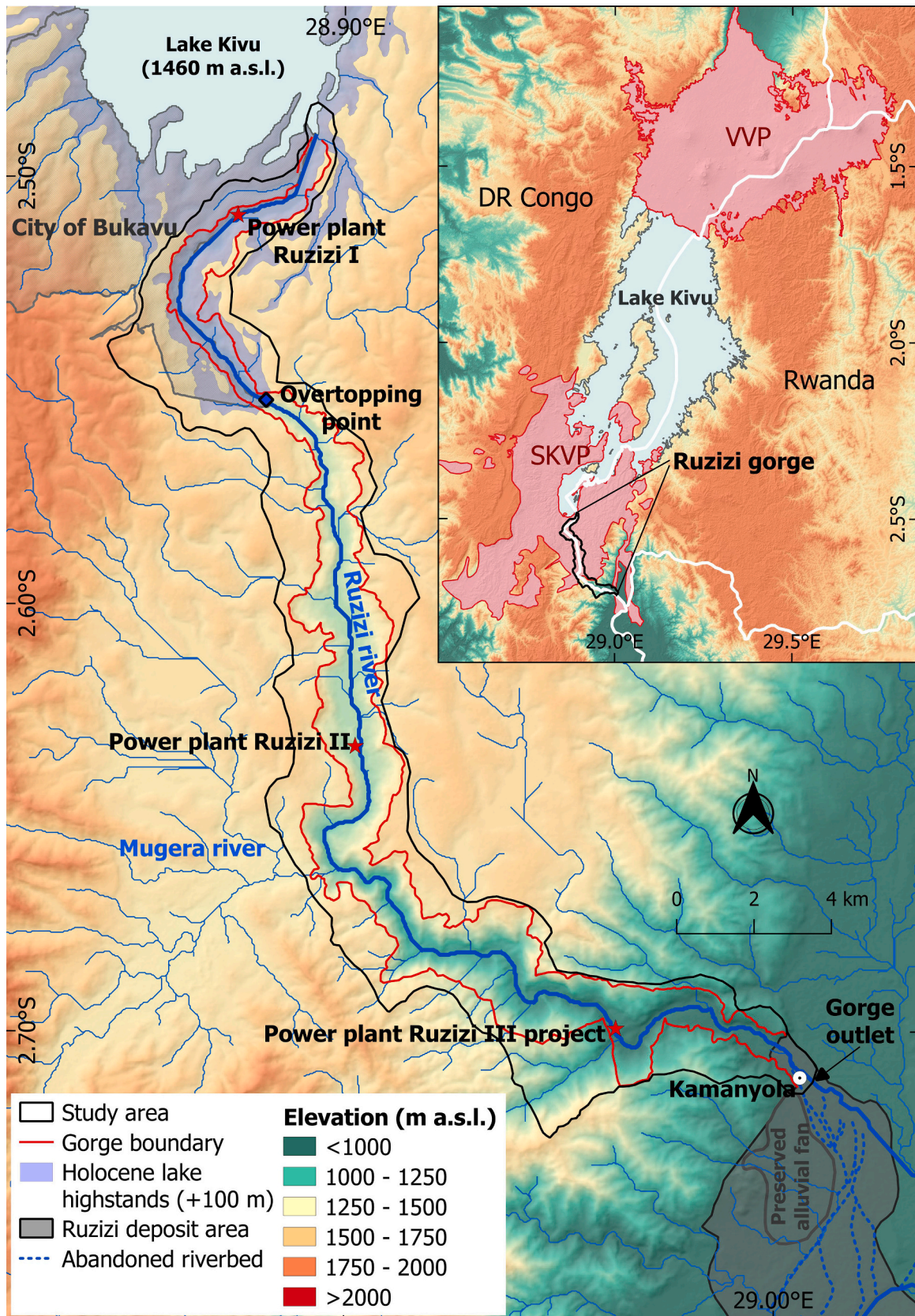
Fig. 1. Overview of the study area. The Ruzizi gorge is situated along the border between DR Congo and Rwanda. Blue lines represent the drainage network. VVP: Virunga Volcanic Province. SKVP: South Kivu Volcanic Province. The overtopping point, i.e., the location where Lake Kivu started draining southwards, is positioned where the overall direction of drainage of the Ruzizi River tributaries changes from north to south, and the lake shoreline at the highstands level converge towards a narrow section of the gorge. Limits of the preserved alluvial fan delineated at the outlet of the gorge and the abandoned riverbed are from Ilunga and Alexandre (1982). Topographic info is from the 1 arc sec ASTER Global Digital Elevation Model (https://lpdaac.usgs.gov/products/astgtmv003/, last access: 22/01/2022).
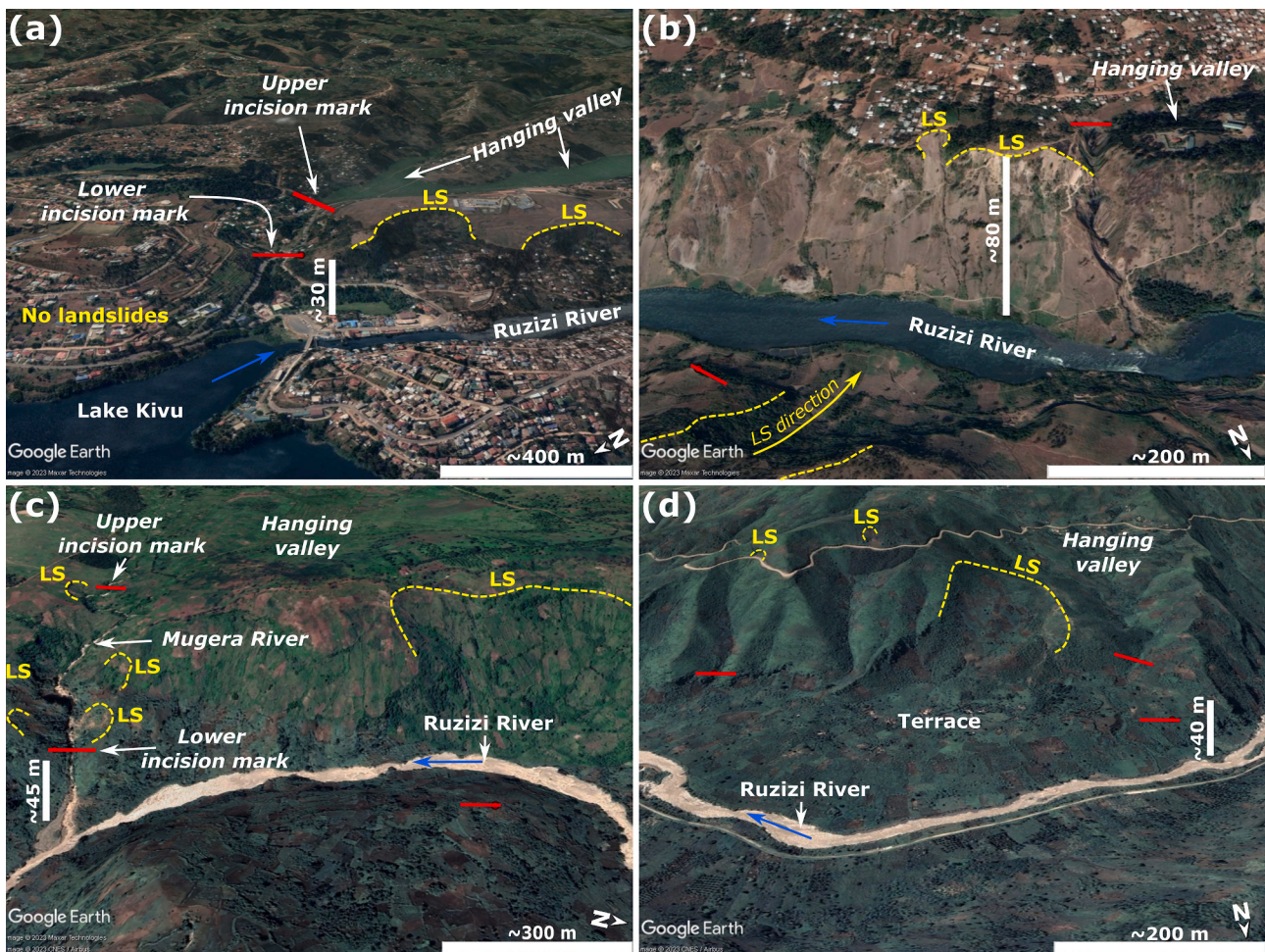
Fig. 2. Examples of incision marks and depths in the Ruzizi Gorge in © Google Earth imagery. Incision marks are depicted by red lines. Landslides (LS) headscarps are indicated in yellow. Blue arrows indicate the Ruzizi River flow direction. (a) Upper and lower incision marks along a tributary at the entrance of the upstream reach of the gorge (2.493°S, 28.896°E). The two incision marks indicates the incision dynamics of the tributary. For the lower incision mark we can assume that it is associated with the sole role of the gorge formation. For the upper mark, this can be questioned. This upper mark, and similarly the upper marks for other tributaries, was therefore not included in the incision depth analysis. (b) Incision mark (2.554°S, 28.879°E) along the tributary whose confluence with the Ruzizi River is located at the overtopping point (Fig. 3b). (c) Lower and upper incision marks (2.663°S, 28.895°E) along the Mugera River (Fig. 3b). (d) Tributary and terrace incision marks (2.696°S, 28.981°E) in the downstream reach (Fig. 3b).

age of the deep-seated landslides based on morphological features and signs of activity of the landslide. Landslides with fresh/new morphological features visible on the 1959 aerial photographs (Table 1) or more recent data were considered as *recent*. Those recognised with a clear and relatively well-defined morphology on aerial photographs from 1959, but without any major traces of recent activity were classified as *old*. The landslides with an altered morphology on aerial photographs from 1959 that show less defined features and/or features modified by soil erosion and other non-landslide processes were classified as *very old*. All shallow landslides were classified as recent processes. For recent landslides, the year of occurrence was determined based on the year of the image/photograph in which the landslide was first observed (following a similar methodology as Guzzetti et al., 2012). The activity period was determined based on the dates of the images/photographs on which the landslide present fresh traces of activity.

It is essential to analyse the completeness and representativeness of the inventory in an area where climatic, geomorphological and demographic conditions predispose to landslide disappearance over time (Guzzetti et al., 2012; Malamud et al., 2004; Van Den Eeckhaut et al., 2007). To do this, landslide frequency area distribution statistics are often used (Malamud et al., 2004; Tanyaş et al., 2018; Van Den Eeckhaut et al., 2007). In this study, we used the maximum likelihood estimation

of the inverse gamma distribution to facilitate comparison with other studies (e.g., Depicker et al., 2020; Van Den Eeckhaut et al., 2007). We used the Kolmogorov–Smirnov test to assess the goodness of fit of the frequency-area distribution to the inverse gamma function (following a similar methodology as Depicker et al., 2020).

3.2. Landslide displacements

We quantified horizontal and vertical ground displacements of landslides over the whole Ruzizi Gorge. We measured horizontal displacements by applying automated pixel tracking on three orthorectified, very-high-resolution stereo and triplet Pléiades satellite images spanning a 5.5-year period (03/2013–07/2018; Table 1). We performed Photogrammetric processing of the Pléiades images (bundle adjustment, topographic surface reconstruction and orthorectification) in MicMac (Rupnik et al., 2017), by using twenty-seven ground control points (GCPs) that were located via differential Global Navigation Satellite System (dGNSS) between 2014 and 2018 in the study area. The accuracy of the dGNSS locations was 7.5 mm for the horizontal component and 16.5 mm for the vertical component. These uncertainties relate to the internal precision of the measurement, field conditions, and data postprocessing (Nobile et al., 2018; Samsonov et al., 2020). We used a co-

Table 1

Key data sources used in this study and the information derived from them. B: boulder characteristics, D: landslide displacement, DEM: digital elevation model, DSM: digital surface model, I: landslide inventory, L: lithology, LU: land use, N.A: Not applicable, P: topographic profiles, RI: river incision traces, RP: river longitudinal profile, RS: rapid sections, T: topographic factors, UAS-SfM: unoccupied aircraft system – structure from motion.

Data	Year	Scale and resolution	Associated information	Source
Historical aerial photographs stereo analysis	1959, 1973	~1:40000	I, LU	RMCA, this study
Orthomosaics from historical aerial photographs	1959, 1973	1 m	I, LU	RMCA for 1973, Depicker et al. (2021b) for 1959
Geological map of Nyangezi	1977	~1:40000	L	Villeneuve, 1977
Google Earth images	2003–2020	0.3 to 0.6 m	I, L, RI, RS	©Google Earth
ASTER GDEM	2011	30 m	P, T	METI and NASA
DSM and related hillshade from TanDEM-X	2013	5 m	I, L, RI	Albino et al., 2015
Pléiades panchromatic images	03/2013, 07/2013, 06/2018, 07/2018	0.5 m	D, I, LU	Airbus
DSM and hillshade from (tri-) stereo Pléiades	Idem	2 m	D, I, RI, RP	This study
UAS-SfM orthomosaics from Pléiades	Idem	0.08 m	D	This study
Field observations	2015–2021	N. A	B, I, L, LU, RI, RS	This study

alignment workflow to reduce registration errors between epochs (Cook and Dietze, 2019). We used COSI-Corr software package (Leprince et al., 2007) to perform automated pixel tracking on the 0.5 m resolution Pléiades orthomosaics. We used decreasing windows sizes (from 512 to 32 pixels) and sixteen pixels steps to measure the east–west (EW) and north–south (NS) components of the surface displacement. We estimated the vertical displacements from vertical difference on 2-m resolution DSM made from the stereo and tri-stereo pairs.

3.3. Landslide frequency and mobilization rate

To explore the short- and long-term spatio-temporal relationships between landslide occurrences and lithology, rejuvenation by bedrock incision and environmental changes, we compared (1) the number and area of landslides and (2) the landslide frequency [#landslides/km^2/y] and mobilization [m^3/km^2/y] rates for the 2003–2020 and pre-1959 periods. For the pre-1959 period, which represents the long-term evolution of the landscape, we assume a duration of 10 Ka considering the direct relationship between the pre-1959 landslides and the gorge formation (Dewitte et al., 2021).

The landslide frequency rate was calculated by dividing the number of landslides by the study area and by the duration of the observation period (Broeckx et al., 2019). We used the same principle to calculate the landslide mobilization rate (LMR), but the number of landslides was substituted with the sum of the landslide volumes (Broeckx et al., 2020). The volume of each landslide was approximated using empirical relationships between landslide source area *(A)* and the observed volume compiled by Larsen et al. (2010). For recent landslides, we used the relationship calibrated for soil landslides in Uganda *"V$_S$"* (Eq. (1a)), because of the geographical proximity and large environmental

similarity. For the pre-1959 landslides, we used the relationship calibrated for the deep-seated landslides *"V$_D$"* (Eq. (1b)).

$$V_S = 10^{-0.40} \times A^{1.22} \tag{1a}$$

$$V_D = 10^{-0.73} \times A^{1.35} \tag{1b}$$

The calculation was performed considering (1) the whole study area, (2) each lithology class, (3) the area rejuvenated by the bedrock incision and the relict area and, (4) each land use class. However, for each land use class, it was only carried out for the 2003–2020 period, as information on the land use of the pre-1959 period is not available.

3.4. Bedrock incision pattern

The river incision depth associated with the gorge formation was determined from the difference between the elevations of the riverbed and relict incision traces such has hanging tributary valleys (Fig. 2). Relict incision traces were identified based on field observations and satellite data (Table 1). To avoid the influence of disturbances from hillslope processes that occurred after the gorge formation, only incision traces located outside landslides were considered. Traces on threshold hillslopes associated with a relatively large widening of the gorge were also not considered. The river rapids were also mapped. The morphology of the tributaries was compared with the incision traces to complete the determination of the incision depth. The average hillslope angle in the areas outside the landslides on either side of the river over 1 km segments were projected onto the longitudinal profile of the river, after calculating the average angle for hillslopes adjacent to each segment (e. g., Larsen and Montgomery, 2012). The same segments were used for the maximum elevation of the gorge boundary and the bounding ridges.

The most detailed lithological information of the study area has been obtained from the geological map of Nyangezi (Villeneuve, 1977) that was establishsed on a regional scale (Table 1). Here, we improved the lithology delineation extracted from this map with field observations and interpretation of satellite products (Table 1).

To better constrain the timing of the gorge formation, we reconstructed paleo-discharges associated with the transport of large boulders that are present in the deposit area formed at the gorge outlet (Ilunga, 1984; Fig. 1). The presence of these boulders makes it the only proxy from which we could infer the (extreme) discharges and hence the possible pace of incision. Detailed information on the reconstruction of these discharges is given in the supplementary material (see Appendix A).

3.5. Human-induced environmental change

Land use mapping and diachronic analysis were performed for the 1959–1973 and 2003–2020 periods. It was done based on orthomosaics of aerial photographs from 1959 and 1973 for the 1959–1973 period (Table 1). The 1959 orthomosaics were created by Depicker et al. (2021b). We produced a 1973 orthomosaic following the same method. For the 2003–2020 period, land use mapping was carried out manually based on very-high resolution-Pléiades images (2013), Google Earth imagery and field observations (Table 1). Three land use classes were considered: woodland, cropland and grassland, and built-up area. For the period 2003–2020, we differentiated built-up density into three distinct categories based on density levels: high-density, medium-density and low-density. An area with a built-up area of ≥70 % or more was considered as a high-density built-up area, an area with a built-up area between 30 % and70% was categorised as a medium-density built-up area, and an area with <30 % of built-up area was categorised as a low-density built-up area.

3.6. Recent landslide distribution and landscape dynamics

We performed bivariate statistical analyses to unravel the relation between recent natural and human-induced landscape dynamics and recent landslides, i.e., slope instabilities that have occurred between 2003 and 2020. These landslides were considered as the dependent variable in our analysis. The explanatory variables were topographical factors (slope angle, elevation, and aspect), lithology, the presence or absence of landscape rejuvenation by bedrock river incision due to the gorge formation, 2003–2020 land use and pre-2003 landslides. The topographic factors were derived from the ASTER GDEM with a 30 m spatial resolution. Jacobs et al. (2018) demonstrate that this resolution is ideal for the analysis of topographic factors for landslide studies in the region. Only the 2003–2020 land use was used because it corresponds to the period of the slope instabilities used as dependent variable. The pre-2003 landslides were used as explanatory variable to unravel the influence of the existing landslides on the occurrence of other landslides.

To avoid spatial autocorrelation, we manually selected one point per landslide depletion area (e.g., Maki Mateso et al., 2023). Since ASTER GDEM provides topographic information from 2011, the slope angle value of each deep-seated landslide observed before that year was calculated using a point taken outside the landslide area on a nearby part of the hillslope that showed topographic conditions and that likely represented the conditions prior to landsliding (e.g., Maki Mateso et al., 2023).

Comparisons were then made between the values of each explanatory variable for the landslide points and the entire non-landslide area on the hillslope. The Ruzizi River and its plain were discarded from the analysis to avoid the inclusion of flat areas that would bias the analysis (e.g., Depicker et al., 2020). To determine the association between these variables and the occurrence of landslides, the Chi-square test was applied with a 95 % level of confidence (e.g., Jacobs et al., 2017). The variables for which an association was found were classified in a set of bins from which a frequency ratio was calculated (Lee and Pradhan, 2007).

We computed a susceptibility index by summing all the frequency ratio values of all explanatory variables at each pixel (Kirschbaum et al., 2012). We calculated the area under the curve (AUC) of the receiver-operating-characteristics curve (ROC) to validate the model (e.g. Depicker et al., 2020). In general, the model is considered acceptable if the AUC > 0.7 (Hosmer et al., 2013). 70 % of the landslides were used to train the model and 30 % to validate it (e.g., Broeckx et al., 2018).

4. Results

4.1. Natural and human-induced environment of the Ruzizi gorge

The modern longitudinal profile of the upper Ruzizi shows two contrasting bedrock channel reaches with similar and uniformly distributed narrow valley widths. The upstream 20 km of the gorge have an average slope gradient profile of 0.004 m m^{-1}, whereas the other 20 km downstream have an average slope gradient of 0.023 m m^{-1} (Fig. 3). This clearly steeper downstream reach corresponds to a knickzone where the majority of the knickpoints are located. Many knickpoints are associated with the presence of small, localised rapids where bedrock outcrops are quite often present together with large, apparently rarely mobile, boulders (Fig. 3b). When considering the rejuvenated landscape, the average hillslope angle (Fig. 3a) is higher in the downstream reach (27°) than in the upstream reach (20°).

The main knickpoint that marks the transition between these two reaches formed within the volcanic rocks. These rocks dominate in the upstream reach, while the downstream reach is dominated by metasedimentary rocks (Figs. 3a and 4a). The metasedimentary rock section that we identified in the upstream reach (from 11 to 17 km from the river's initiation point) corresponds to a new set of lithological information that was not mentioned on the reference geological map of the region (Villeneuve, 1977). The overtopping point, located in the volcanic rocks, is not associated with a specific knickpoint.

We identified 39 incision marks on the hillslopes along the river (Figs. 2; 3b). The average incision depth is ~80 m in the upstream reach (max of 111 m) and ~58 m (max of 93 m) in the downstream reach. Overall, the incision trends show a paleo river longitudinal profile that is similar in terms of steepness to that of the modern situation (Fig. 3b).

The longitudinal profile of the Mugera River exhibits a knickpoint that corresponds to an incision depth of 220 m (Fig. 3b). This knickpoint is at an elevation that is similar to the incision marks in the upstream reach. The longitudinal profile of the Mugera River upstream of its main knickpoint is similar to the longitudinal profile of the upstream reach of the Ruzizi River. It is also similar to the profile of the tributary river at the overtopping point (Fig. 3b).

We have identified several meter-scale boulders in the deposit area apex (Fig. 1). The paleo-discharge required for transport of these volcanic rock boulders is estimated to ~5000 m^3 s^{-1} (see Appendix 1).

Between 1959–1973 and 2003–2020, the most striking difference in land use lies in the increase in built-up areas (Fig. 5). Initially located on very few locations along the very upstream part of the study area, the built-up areas now cover more than ~26 % of the study area. This increase in built-up areas was mostly done at the expense of the croplands and grasslands (Fig. 5a and c). Also, not only has the total area of woodland decreased, but there has also been a redistribution of the remaining woodlands over the area.

4.2. Typology and characteristics of old and recent landslides

Our multi-temporal inventory contains 385 landslides (Fig. 4), with surface areas ranging from 30 m^2 to 1.80 km^2 (Table 2). Landslides cover 24 % of the total study area, with an overall density of 4.2 landslides per km^2. These values are higher when considering only the gorge itself. There, landslides cover 48 % of the landscape, with an overall density of 7.1 landslides per km^2. The pre-1959 landslides are concentrated mostly in the upstream reach while the 2003–2020 ones are more evenly concentrated (Fig. 4). The inventory contains ~75 % of flow-like landslides (earthflows, flowslides, debris flows and debris avalanches) and ~ 25 % of slides (rotational and planar slides; Figs. 4, 6, 7; Table 3). In terms of area, however, rotational slides alone account for ~64 % of the total landslide area, followed by planar slides (~13 %). Flow-like landslides on the other hand represent about ~23 % of the total landslide area (Table 3, Fig. 7a). Slides are mainly present in the upstream reach in both volcanic and metasedimentary rocks. The flow-like landslides are mainly concentrated in the metasedimentary rocks of the downstream reach (Figs. 4, 6; Table 3).

Many large landslides and a few small shallow landslides are connected to the river channel. For example, the convergence of two large landslide accumulation zones is at the origin of the formation of a dam lake (Fig. 4a, c). This dam lake is only partially incised, which explain the presence of rapids (Fig. 3b) on which the Ruzizi II power plant is currently located. Landslides are clear provider of river material, as attested by the presence of many large and apparently rarely mobile boulders in the channel. Where they cluster, these boulders contribute to the formation of rapids and anchored knickpoints (e.g., Whipple et al., 2022).

In terms of landslide age, we can make a distinction between two major groups: (1) recent landslides that have occurred and/or were reactivated over the past 60 years and (2) (very) old landslides (pre-1959), whose morphology is sometimes altered by erosion. The pre-1959 landslides are generally much larger and deeper than the recent ones and are mainly of the slide type. The recent ones are mostly flow-like landslides and are mostly shallow and with small dimensions (Tables 2 and 3; Fig. 7). Landslides with an area ≥ 10 ha are often considered as large (Crosta et al., 2018; Pánek et al., 2019); ~15 % of the inventoried landslides belong to this category and >85 % of them date from the pre-1959 period (Fig. 3c; Table 2). Observations made on the
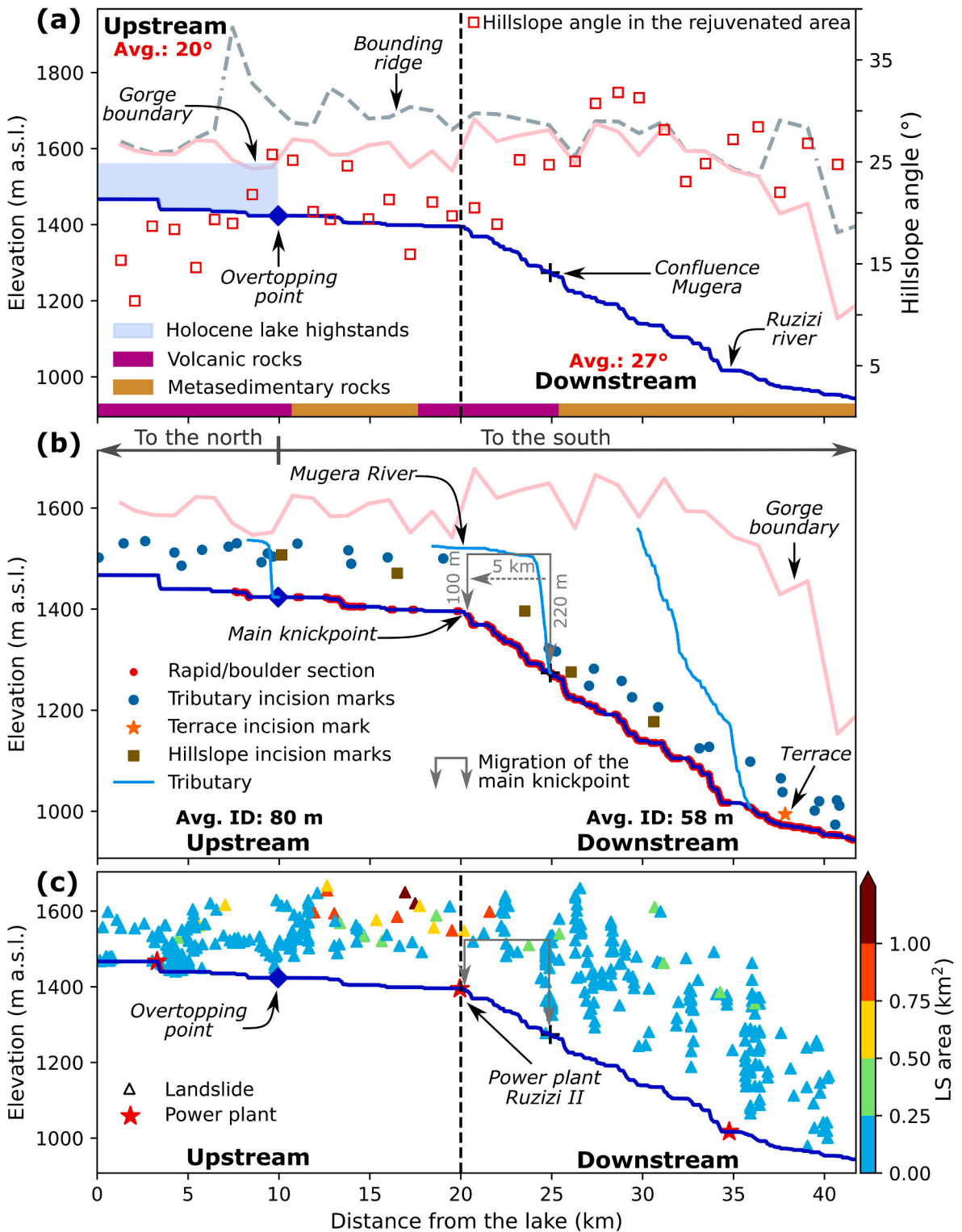
Fig. 3. Distribution of hillslope angles (a), incision marks (b) and landslides (LS) area (c) in the relation to the modern longitudinal profile of the Ruzizi River and its main tributaries, the gorge boundary, and the lithology. The rapid/boulder sections, the overtopping point, the main knickpoint and its migration, the main confluence (confluence Mugera), and the power plants are also represented. The two flow directions of the drainage system are indicated by the arrows at the top of (b). The lithology is indicated at the bottom of (a). Each triangle in (c) represents a landslide of the indicated area (based on the colour bar). The upstream and downstream reaches are separated by the black dashed line (a and c). The average upstream and downstream slope angles (Avg.) in the rejuvenated landscape outside the large landslides are shown in red in (a). The direction of the migration of the main knickpoint is indicated by the dashed grey arrow. Values of its extent are also given. Avg. ID: average incision depth.
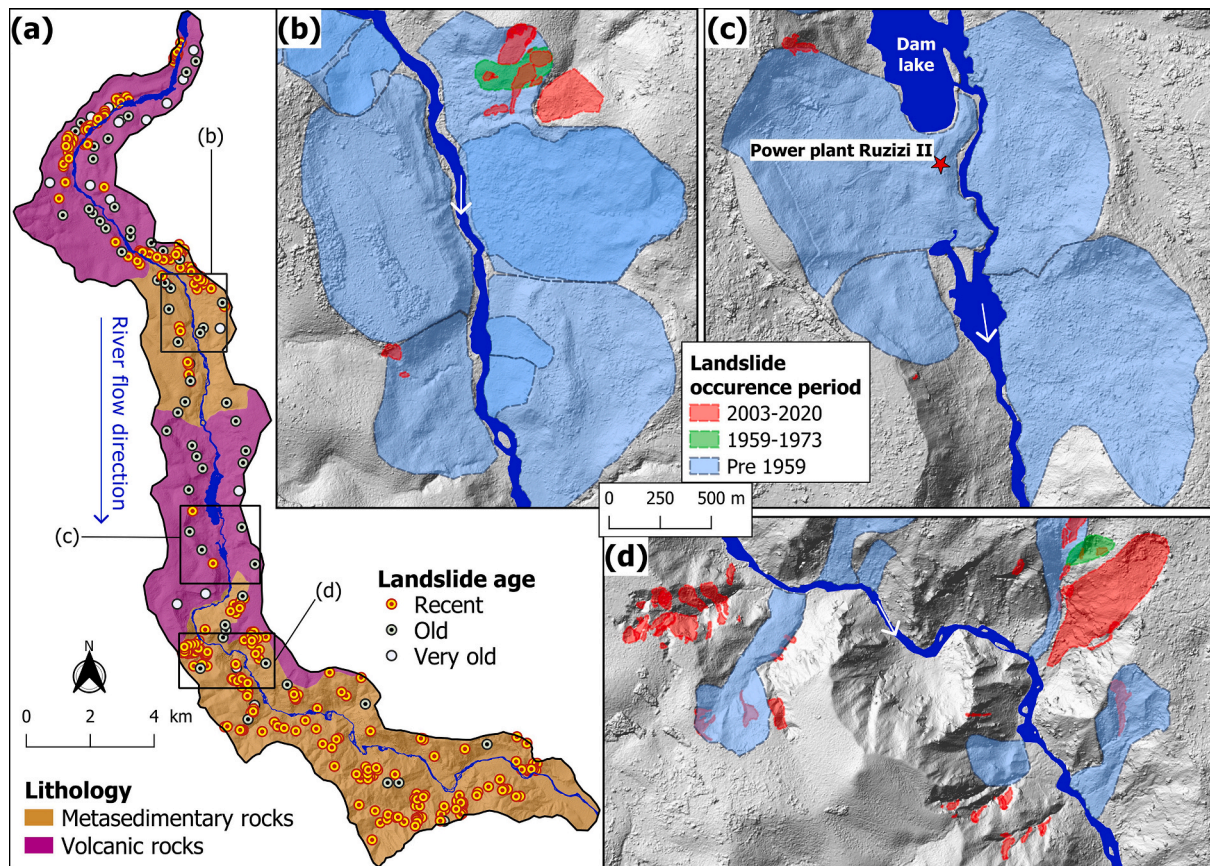
Fig. 4. Landslide inventory in the study area. (a): reference points at the source areas of the landslides with the lithology in background. (b, c, and d): zooms in three locations according to the lithology pattern. The landslides are coloured by age categories. Hillshade is derived from the (tri-) stereo Pléiades DEM (Table 1). White arrows indicate the river flow direction. Lithology is updated from Villeneuve (1977, see text for explanation).

images from 2003 to 2020 show that small flow-like landslides are typically recolonized by vegetation after 2 to 3 years. The inverse gamma distribution, fitted on the area-frequency distributions of the landslides yielded p-values of 0.001, 0.258 and 0.364 and power-law decay of −1.118, −1.707 and −0.986 for the whole inventory, the 2003–2020 and pre-1959 landslides, respectively (Fig. 7d).

4.3. Landslide distribution and dynamics in the Anthropocene

For the 2003–2020 period, the frequency ratio values stress landslide favourable controls (Table 4) as: (1) slopes >20° with higher control from 30°, (2) the area rejuvenated by bedrock incision, (3) the metasedimentary rocks, (4) the elevation classes between 1200 m and 1500 m, (5) the cropland and grassland areas, (6) the north slope aspect, and (7) the presence of the pre-2003 landslides. The slope distribution in the significant land use classes reveals that the largest portions of the recent landslides occur on slopes steeper than what is found in the whole landscape (Fig. 8). It is noteworthy to mention that landslides in cropland and grassland areas occur on slopes that are steeper than in built-up areas. This dominant role of the slopes, combined to the one of the metasedimentary rocks and the presence of the pre-2003 large landslide main scarps, are clearly highlighted in the susceptibility model (Fig. 9). The downstream reach of the gorge is clearly the region which is currently the most impacted by the occurrence of new landslides.

Only one partial reactivation is detected for the large landslides from our analysis of the ground surface displacement over the 2013–2018 period (Fig. 10b). Horizontal motions up to 8 m are principally detected in the middle to upper part of the landside and are associated with partial reactivation of the main scarp that occurred in 2016 according to local farmers. Other displacements were measured in four recent, and

much smaller, landslides. For one of them the motion pattern corresponds to that of an active rotational slide (Fig. 10c). All five landslides are located in the rejuvenated landscape in metasedimentary rocks, where grasslands and croplands represent the main land cover (Figs. 4a, 5a, 10a).

4.4. Landslide mobilization rates

Overall, the pre-1959 landslide source areas are larger, but less numerous than those identified during the 2003–2020 period (Fig. 11). However, when the LMRs are considered, an opposite pattern is observed. More specifically, this significantly higher LMR for the recent period is principally observed for the landslides occurring in the rejuvenated landscape in the downstream reach. This difference in LMRs between the two periods is much less pronounced in the upstream reach.

The recent landslides are mainly concentrated in cropland and grassland areas, both in term of numbers and source area. Landslides in these areas account for ∼87 % of all landslides and have a mobilization rate that is ∼9 times higher than landslides in other land use classes combined (Fig. 11).

5. Discussion

5.1. The Ruzizi Gorge, a landslide hotspot in a landslide prone region

The multi-temporal inventory provides detailed information on landslides that was not available in previous works (Depicker et al., 2020; Dewitte et al., 2021; Monsieurs et al., 2018). The combination of multi-temporal high-resolution data and intensive field work has been crucial in establishing such a detailed landslide inventory (e.g., Korup,
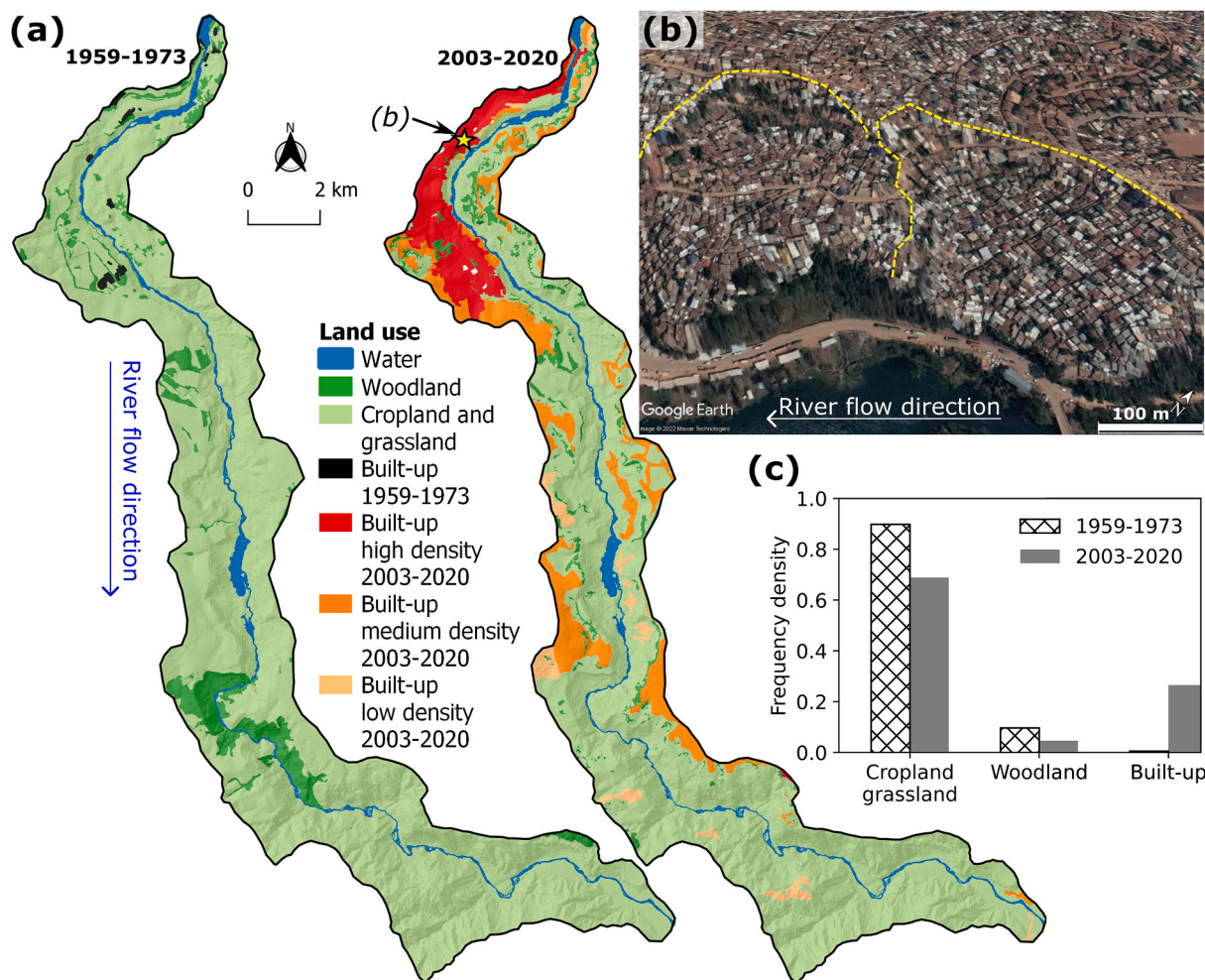
Fig. 5. Land use in the study area. (a): land use for the 1959–1973 and 2003–2020 periods. (b): example of a high-density built-up area on two large old landslides (delineated in yellow dashed lines). These landslides are located with a star in Fig. (a). Image © 2022 Google Earth. (c): percentage of land use classes in the two periods.

Table 2
Landslides (LS) area statistics for the different occurrence periods.

Period	# LS	#LS ≥ 10 ha	Min area (ha)	Max area (ha)	Average area (ha)
2003–2020	281	5	0.003	42.9	0.9
1959–1973	14	2	0.70	18.9	6.7
Pre 1959	90	49	0.26	180.4	24.4

2006; Kubwimana et al., 2021), especially for the period 2003–2020 where landslides have a higher representativity in the inventory.

The concentration of large and (very) old landslides within the gorge is clearly high in comparison with other river reaches investigated in the North Tanganyika-Kivu rift region (e.g., Depicker et al., 2020; Kubwimana et al., 2021; Maki Mateso et al., 2023). With ~48 % of the rejuvenated landscape impacted, this clearly places the Ruzizi Gorge as a regional hot spot for large landslides. Yet, it should, be mentioned that (1) the largest landslide (1.8 km^2) is here much smaller than the largest found in the region (several landslides >10 km^2, Dewitte et al., 2021; Kubwimana et al., 2021) and (2) that smaller landsides are also frequent along (mostly the downstream reach of) the Ruzizi River.

Both recent and (very) old landslides show frequency-area distributions that differ from those found for the whole North Tanganyika – Kivu rift region by Depicker et al. (2020). The power-law decay exponents are clearly greater in the Ruzizi Gorge, highlighting here a stronger

dominance of large size landslides. This further show the specific setting of the Ruzizi Gorge.

5.2. A four-step gorge incision – landslide occurrence interaction model

Our analyses allow us to reconstruct the origin and evolution of the landsides in four key steps, with respect to the formation of the Ruzizi Gorge over the last 10 ka (Fig. 12).

5.2.1. Step 1: an extremely rapid incision and the birth of large landslides
The rapid overall incision of the gorge is evidenced by (i) the modern longitudinal profile of the river, which has an overall steepness similar to the profile at the time of the overflow initiation; (ii) the main knickpoint, which has migrated 5 km northward over the past 10 ka; (iii) the width of the valley, which is narrower and relatively uniform despite the presence of contrasting lithologies; and (iv) the fact that the mean hillslope angles in the rejuvenated landscape upstream and downstream correspond to threshold slopes (Baynes et al., 2015; Depicker et al., 2021a; Korup and Weidinger, 2011; Schanz and Montgomery, 2016; Whipple et al., 2022). Overtopping, formation of waterfalls, plucking and knickpoint retreat are all processes that can be invoked in bedrock river incision (Anton et al., 2015; Cook et al., 2013; Fan et al., 2018; Lamb and Fonstad, 2010). Such processes can be associated with sometimes extremely high incision rates and the occurrence of extreme peak discharges. The presence of large volcanic rock boulders in the
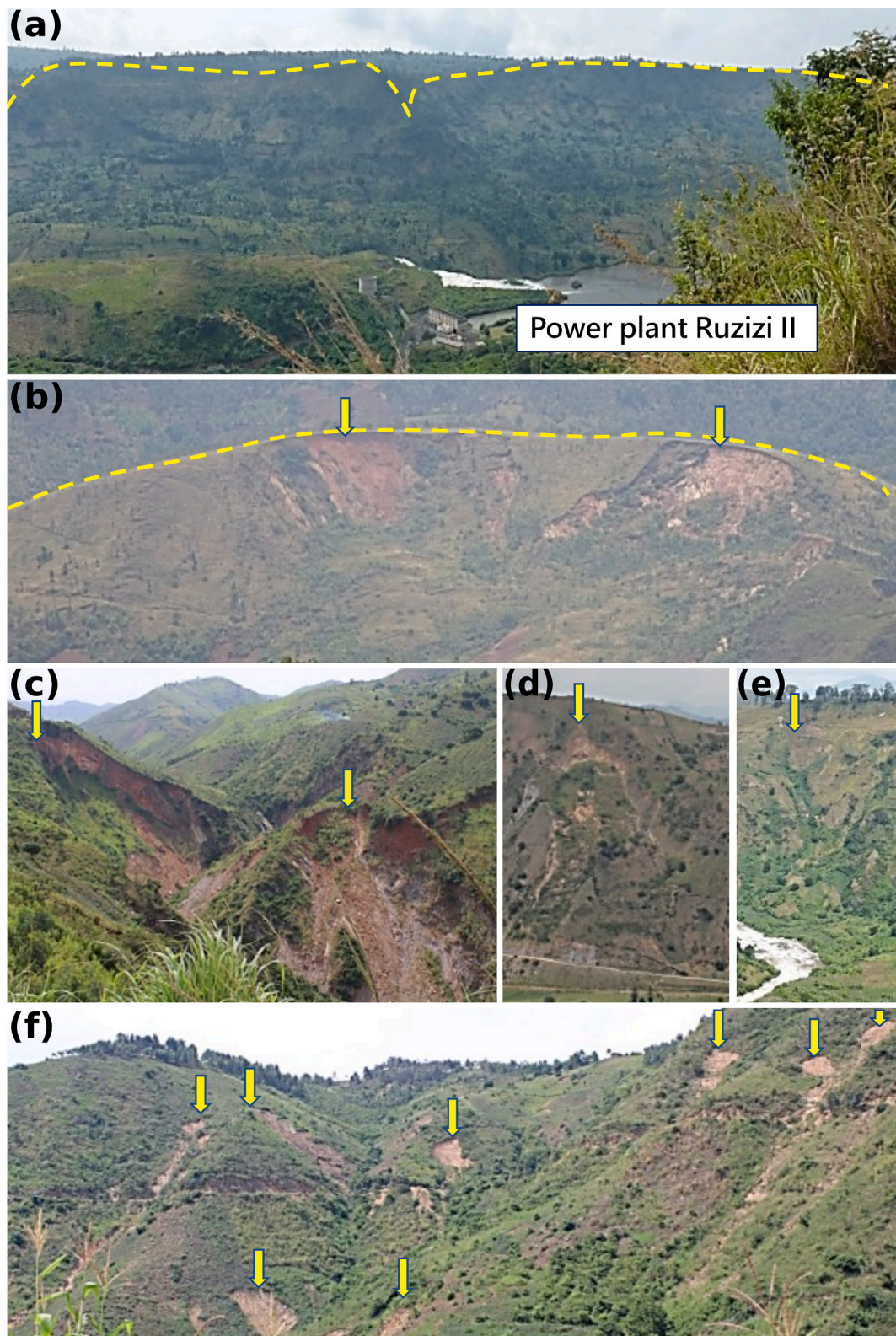
Fig. 6. Examples of landslide processes in the Ruzizi Gorge. (a): old rotational slides at level of the power plant Ruzizi II (photo taken in June 2016). The main scarp height is >100 m. (b): recent slope instabilities at the main scarp of an old large rotational slide (photo taken in September 2020). (c): recent rotational landslide (left) and flowslide (right; photo taken in February 2021). (d): recent flowslide (photo taken in February 2021). (e): earthflow (photo taken in June 2016). (f): cluster of debris avalanches and debris flows triggered in December 2020 (photo taken in February 2021). The yellow dotted lines and arrows indicate the main scarp of the old and recent landslides respectively. (a) is located in material from volcanic rocks while the other photos are located in material from metasedimentary rocks. All the landslides in the photos taken in 2021 occurred before 2021.
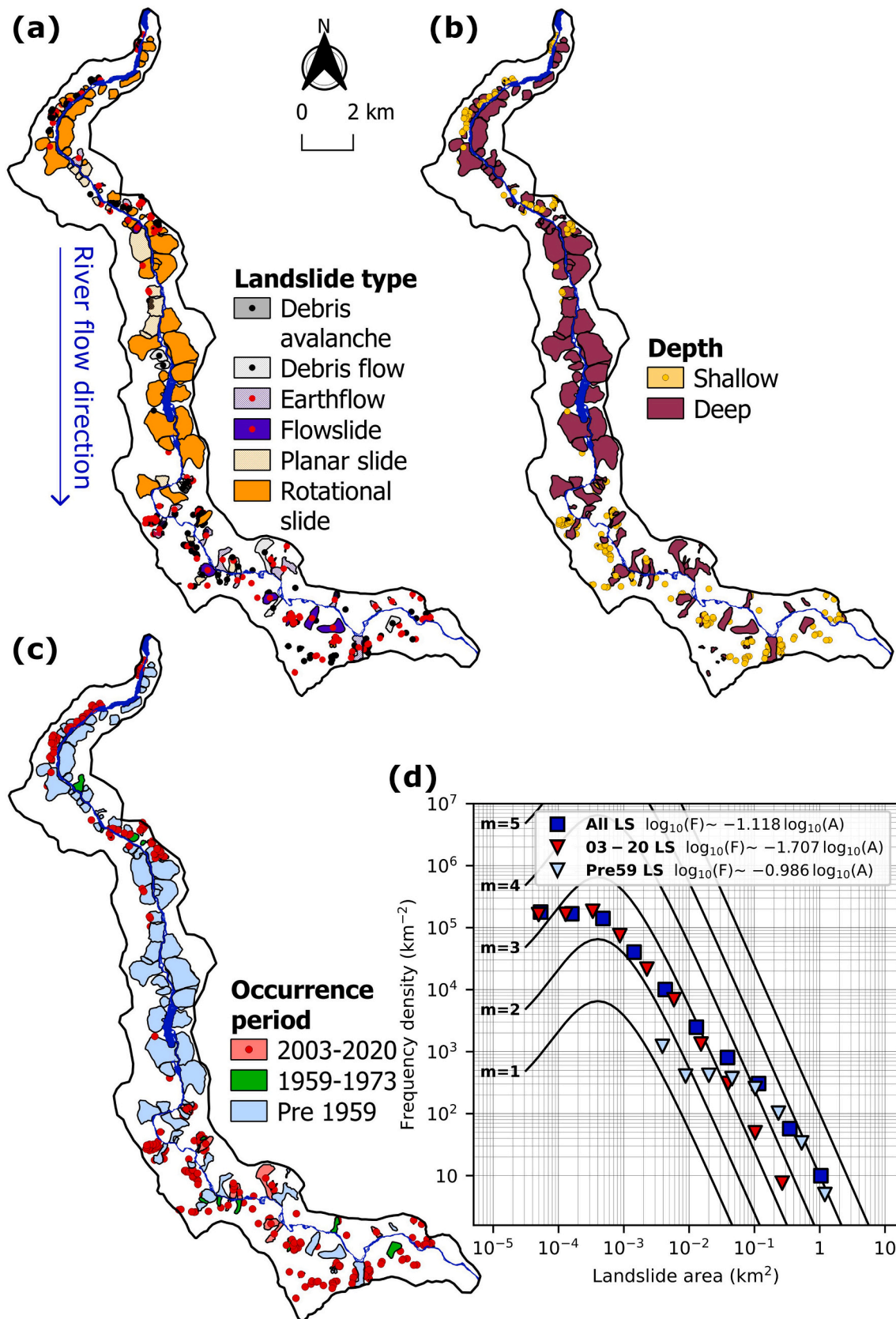
Fig. 7. Landslide processes. (a, b, c): landslide classified by type, depth, and occurrence period respectively. In order to be visible at the scale of the maps, the landslides <25,000 m^2 are symbolized with a dot. (d): landslide frequency density distributions as a function of landslide area for the whole inventory (All LS), the 2003–2020 landslides (03–20 LS), and the pre-1959 landslides (Pre59 LS). The black curves indicate the theoretical distributions for various landslide-event magnitudes (m) of Malamud et al. (2004): m = 2 means an inventory that would contain 100 landslides, m = 3 means 1000 landslides, etc.

Table 3

Landslide numbers and respective percentages of the total landslide area according to the relative age and the depth. RS: rotational slide, PS: planar slide, EF: earthflow, FS: flowslide, DA: debris avalanche. Total type: sum of landslide number or area for each landslide type, Tot C: sum of landslide number or area for each characteristic.

Landslide number								
Characteristic	Type	RS	PS	DA	EF	FS	DF	Tot C
Occurrence period	2003–2020	16	13	112	6	99	35	281
	1959–1973	3	1	–	3	3	4	14
	Pre 1959	47	18	–	9	12	4	90
Relative age	Recent	22	15	112	9	108	39	305
	Old	30	15	–	9	6	4	64
	Very old	14	2	–	–	–	–	16
Depth	Shallow	9	9	96	4	83	30	231
	Deep	57	23	16	14	31	13	154
Total type		66	32	112	18	114	43	385

Landslide area (%)								
Characteristic	Type	RS	PS	DA	EF	FS	DF	Tot C
Occurrence period	2003–2020	1.6	0.9	1.2	0.5	2.4	3.2	9.7
	1959–1973	0.5	0.1	–	1.4	0.6	1.2	3.7
	Pre 1959	62.4	11.9	–	6.1	4.5	1.8	86.6
Relative age	Recent	5.8	1.9	1.2	1.8	3.5	4.4	18.7
	Old	48.0	10.0	–	6.1	3.9	1.8	69.9
	Very old	10.6	0.9	–	–	–	–	11.5
Depth	Shallow	0.2	0.1	0.5	0.0	0.8	0.6	2.3
	Deep	64.2	12.7	0.7	7.9	6.7	5.6	97.7
Total type		64.4	12.8	1.2	7.9	7.5	6.2	100.0

Table 4

Results of the Chi-square test and the frequency ratio analysis for the 2003–2020 period. Frequency ratio values >1.1 (in bold) suggest more favourable conditions for landside occurrence. *: P-value >0.05, **: P-value ≤0.01, ***: P-value ≤0.0001.

Variable	Chi-square	P-value	Class	Frequency ratio
Slope	259.2	***	0–5°	0.09
			5–10°	0.10
			10–15°	0.43
			15–20°	1.03
			20–25°	**1.14**
			25–30°	**1.90**
			30–35°	**3.40**
			35–40°	**2.51**
			> 40°	**2.56**
Slope aspect	11.59	**	315–45° (north)	**1.22**
			45–135° (east)	1.01
			135–225° (south)	1.08
			225–315° (west)	0.70
Elevation	63.3	***	< 1100 m	0.75
			1100–1200 m	0.98
			1200–1300 m	**1.55**
			1300–1400 m	**1.85**
			1400–1500 m	**1.39**
			1500–1600 m	0.86
			>1600 m	0.30
Lithology	54.4	***	Metasedimentary	**1.41**
			Volcanism	0.52
Rejuvenation by incision	64.0	***	Rejuvenated	**1.43**
			Relict	0.46
Pre 2003 landslides	1.5	*	Out landslide	0.96
			In landslide	**1.14**
2003–2020 land use	40.3	***	Woodland	1.01
			Cropland and grassland	**1.21**
			Built-up high density	0.44
			Built-up medium density	0.19

deposit area of the Ruzizi River (Fig. 1) are evidence of past extreme peak discharges (~50 times larger than the current average river discharge). Although the reconstruction of these paleo-discharges is always bounded with relatively large uncertainties, it corroborates the hypothesis of an overall high incision rate period. Such mechanisms are known to be nonlinear, therefore leading to various waves of incision that can nevertheless occur within quite a short period of time, sometimes in a few days (Lamb and Fonstad, 2010). This could explain why, in addition to the highest levels of incision, other incision levels are recorded, such as the one associated with a localised strath terraces in the metasedimentary rocks downstream (Fig. 2d). Note that this terrace, which is not covered by boulders, is the only terrace level that we have observed in the gorge.

In the upstream reach, almost all large pre-1959 landslides are of the same type, with a similar morphology and with similar post-landslide surface erosion marks, suggesting that they occurred within a relatively narrow time window (e.g., Booth et al., 2017). These large and (very) old landslides show no signs of activity. In the neighbour city of Bukavu, surface displacements are clearly detected over most of the body of a landslide of similar type, size, and lithology but with a morphology clearly fresher (Dille et al., 2022). Since the occurrence of this active landslide in Bukavu is estimated to be ~5000 years (Dewitte et al., 2021), we could assume that the old and very old landslides in the gorge are relatively much older. Such hypothesis on the age of the landslides made on one single observation of surface deformation in the region could be questioned. Yet, other studies in other environments have shown that surface deformation can still be detected on thousand-year-old landslides (Booth et al., 2017; Dewitte et al., 2009; Korup, 2006). Similarly, no deformation is detected in the large (very) old landslides in the downstream reach, even though they are of a different type than in the upstream reach. All of this suggests that these large landslides in the gorge occurred fairly quickly after the main incision phase and the associated topographic conditions (Azañón et al., 2005; Burbank et al., 1996; Fan et al., 2018; Yenes et al., 2015).

In the upstream reach, we observe similar landslide types in the two contrasting lithologies. The eastern bank of the gorge is part of a hillslope with similar lithology and elevation differences that extends further to the north along Lake Kivu (Fig. 2a). However, this hillslope
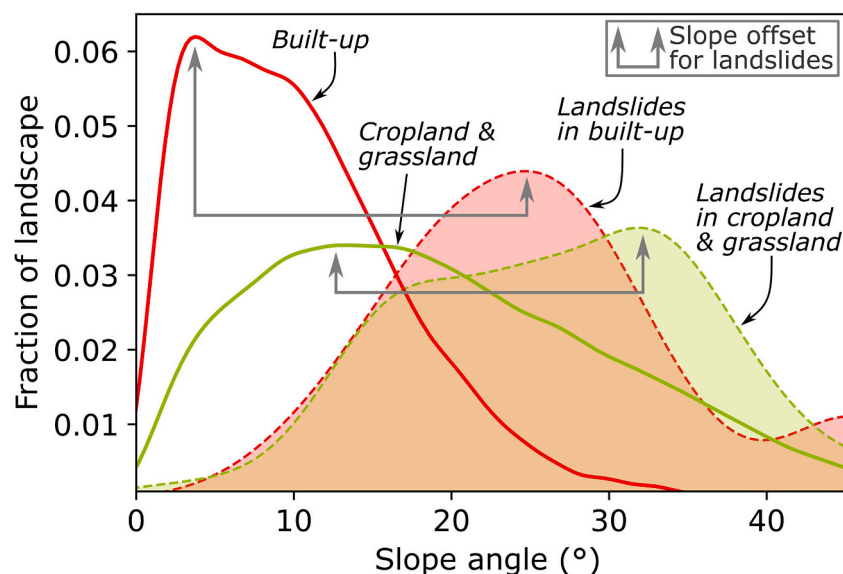
Fig. 8. Slope angle distribution of the whole landscape (without landslides) and landslides in different land use classes during the 2003–2020 period. The slope distribution peaks for landslides are both offset towards slopes steeper than for the whole landscape.

along the lake has not been rejuvenated and no large landslides are observed (Fig. 2a). These observations reveal a dominant role of incision forcing over the lithology, providing further evidence of the rapid incision of Ruzizi Gorge (e.g., Roda-Boluda et al., 2018). The longitudinal profile of the downstream reach is steeper and characterized by more frequent and pronounced knickpoints, as compared to the upstream reach (Fig. 3). In such a topographic context, one could expect a higher concentration of large landslides in this part of the gorge (e.g., Bennett et al., 2016). Yet, we here observed the opposite. Although composed of the same two lithologies, the downstream reach is dominated by metasedimentary rocks that are less weathered and, hence, less prone to deeper (and potentially larger) slope failure (Clarke and Burbank, 2010; Dille et al., 2019; Frattini and Crosta, 2013). In addition, the overall incision wave due to landscape rejuvenation in the downstream reach is less important than in the upstream one (Fig. 3b). This observation suggests that the topographic control due to incision is threshold-dependant and dominates over the lithologic control on the occurrence of large slope instabilities only when a certain incision depth and/or rate is reached.

We cannot ignore that the seismicity in the region has the potential to be at the origin of large landslides (Delvaux et al., 2017; Maki Mateso et al., 2023), although over the last decades no seismically-triggered landslides were observed (Dewitte et al., 2021). As said in Section 5.1, the cluster of large landslides in the Ruzizi Gorge is unique, and if earthquakes played a role in their occurrence, it is likely to be minor; the triggering conditions being highly facilitated by the rapidly formed threshold hillslopes associated with the landscape rejuvenation (e.g., Yenes et al., 2015). Over the past 10 ka, the climate in the region has been relatively similar to the present one, although relatively short periods of drier conditions associated with slight decrease of lake level could have happened, which may have interrupted the flowing of the lake (Felton et al., 2007). The origin of the large landslides associated with climatic variability would therefore be highly hypothetical.

5.2.2. Step 2: large landslide evolution and gorge incision stabilisation

The sudden occurrence of large landslides can deliver important volumes of coarse material into the channel (Ouimet et al., 2007). This material can easily dam the river, whose breaching can lead to subsequent outburst floods (Nibigira et al., 2018), resulting in additional but presumably less deep incision waves. This may explain the presence of the larger range of incision mark depths in the downstream reach

(Fig. 3b).

Once initiated, landslides are likely to continue to grow, with potentially several phases of reactivation, e.g., favoured by the erosion of their toe and the maintenance of a critical slope angle (Booth et al., 2017; Dille et al., 2019; Mackey and Roering, 2011; Mather and Stokes, 2018). Landslide damming, disturbance of longitudinal sediment connectivity and outburst flood can therefore, to some extent, repeat. However, in our study area, the morphological conditions of the gorge in terms of the size of the landsides (Figs. 1, 2, 3, 4, 10a) suggest a relatively quick stabilisation of this process of landslide growth. Indeed, the relief associated with the depth of the gorge as well as the width of the gorge and hence the potential length of travel distance of the landslides are limited. Limited relief and limited travel distance are control factors that are known to limit the landslide size and their reactivation (Iverson et al., 2015; Korup et al., 2007).

At the onset of the gorge, the feedbacks between the hillslopes and the channel are yet highly dynamic. Landslides are active, prone to reactivation, and new large landslides can still occur, potentially in interaction with the subsequent waves of incision associated with the upstream migration of knickpoints. In that context, the channel continuously receives new hillslope material. It is obvious that not all the material delivered by the landslides to the river remains in place (Croissant et al., 2017; Shobe et al., 2021); as attested by the presence of transported boulders in the deposit area (Ilunga and Alexandre, 1982; Fig. 1). These sediment pulses, whose transport can be modulated by the discharge variability associated with the breaching of landslide dams, contribute to reducing the incision over a given length of the river (Ouimet et al., 2007). The export time of these sediments leads to temporal self-reorganisation of the river channel (Croissant et al., 2017). The whole mechanisms associated with the sediment pulses may explain why a larger range of incision mark depths are observed in the downstream reach.

In parallel, large landslides mantle the channel bed upstream and downstream with immobile large boulders, protecting the bedrock from further incision by the river. This process of armouring and its associated negative feedback (Bennett et al., 2016; Mather and Stokes, 2018; Ouimet et al., 2007) is exacerbated by the fact that the river formed at the mouth of a large lake in a tropical climate zone with limited inter-annual rainfall variability and relatively constant climate conditions over the past 10 ka years (Felton et al., 2007). As such, the river does not naturally experience high discharge variation (Muvundja et al., 2022),
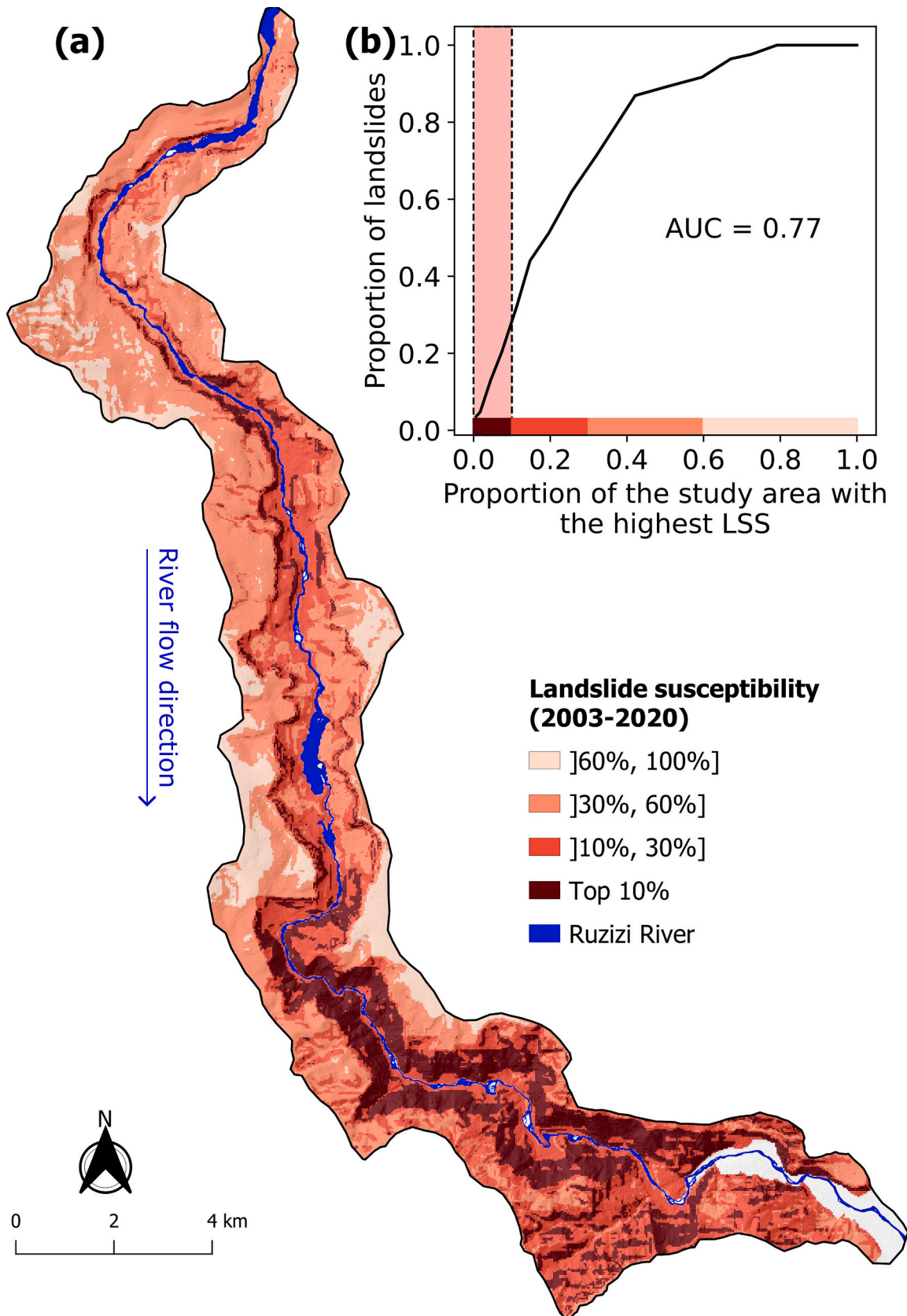
Fig. 9. Frequency ratio-based landslide susceptibility model for the 281 recent landslides that occurred during the 2003–2020 period. (a): overall susceptibility map. (b): prediction rate curve of the model. The 10 % of the study area with the highest landslide susceptibility (LLS) values are highlighted by the pink bar with dashed outline.
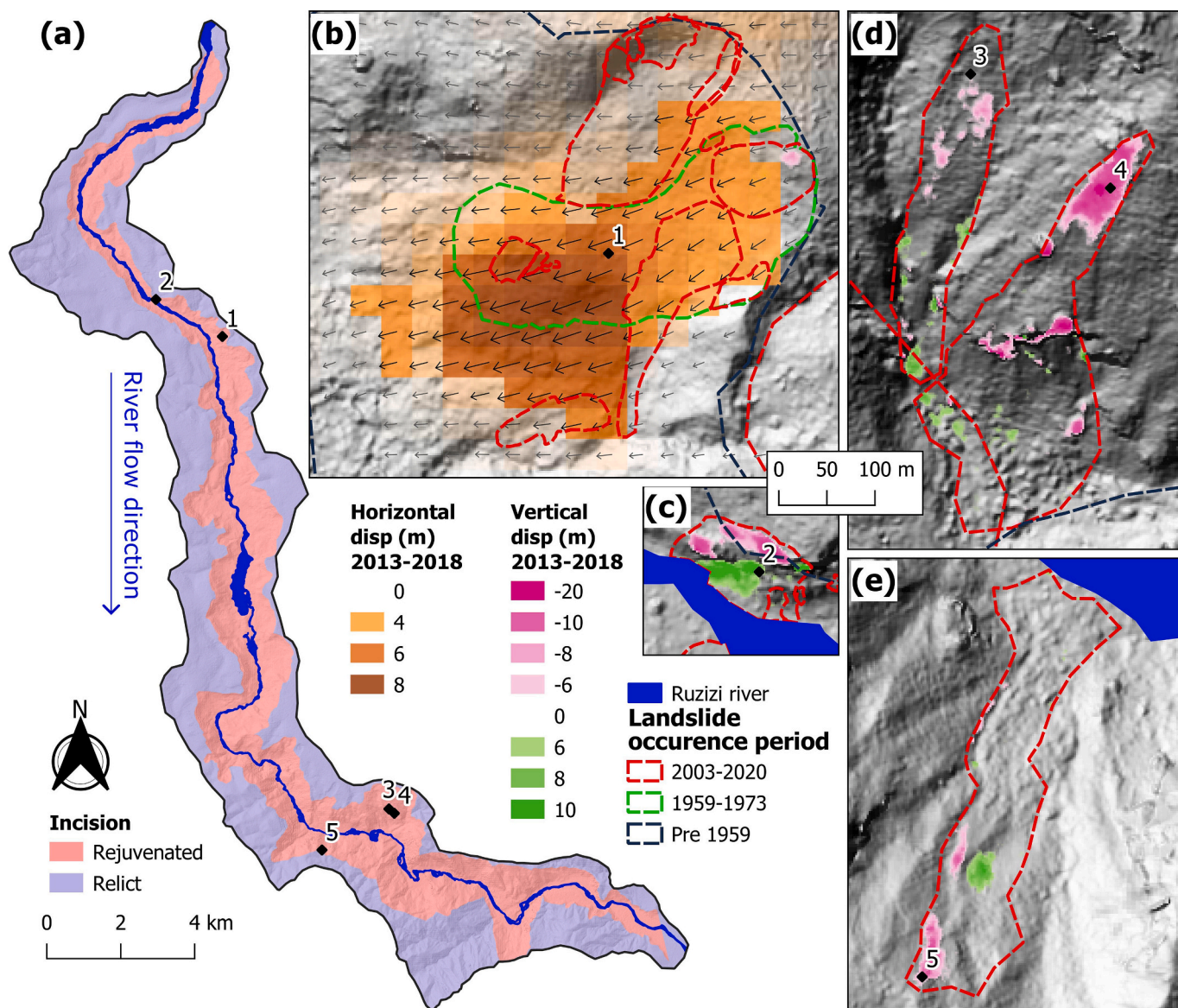
Fig. 10. Measured landslide displacements over the 2013–2018 period from multi-temporal Pléiades images. (a): location of the landslides where displacements were measured with respect to the rejuvenated landscape. (b, c, d): zoom on the respective landslides. Disp: displacement.

and hence associated transport capacities (Shobe et al., 2021). This regularity of the discharge limits the erosion of the landslide toes, therefore contributing to their stabilisation and longevity (Booth et al., 2017).

The average incision depth in the downstream reach of the river is less important than the one of the upstream reach. This is due to the presence of a former valley that existed prior to the initiation of the gorge, resulting in a paleo-topography closer to the base level of the gorge's deposit area. In addition, as armouring and sediment pulses are more present in this reach of the river, we can state that they have contributed to exacerbate this difference in average incision depth.

Several studies have explored these interactions and feedbacks between river incision and landslides that occurred over landscape evolution timescales of tens of thousands of years (e.g., Bennett et al., 2016; Ouimet et al., 2007). Here, these processes haven taken place over a much shorter period. Formed at the mouth of a lake, the Ruzizi River contains at its source a very limited suspended sediment load, and the bedload is absent. Hence, the inherent incision potential of the river is negligible (Cook et al., 2013). This, in addition to the stabilized state of the large landslides, boulder-armoured bedrock, anchored knickpoints

and low discharge variability, are factors that contribute to the current apparent steady state of the gorge incision.

5.2.3. Step 3: the domination of small, high frequency landslides

The hillslopes are affected by small (and mostly shallow) rainfall-triggered landslides. These landslides are favoured by the metasedimentary rocks and landscape rejuvenation. A path dependency is observed on the steep slopes associated with the large landslides that favour the occurrence of more recent instabilities (e.g., Samia et al., 2017). These topographic controls on the occurrence of shallow landslides reveal the complex interactions between slope angle, weathering, and regolith availability. For the same slope angles, the metasedimentary hillslopes could be less prone to shallow landslides, since the overall weathering of the rocks is less intense than what is observed in the volcanic lithology. However, we observe the opposite; which could be explained by favourable hydrogeological and strength characteristics that remain to be investigated (Frattini and Crosta, 2013; Roda-Boluda et al., 2018).

Shallow landslides, in combination with sediment from the small tributaries, contribute to a small progressive downstream increase of the
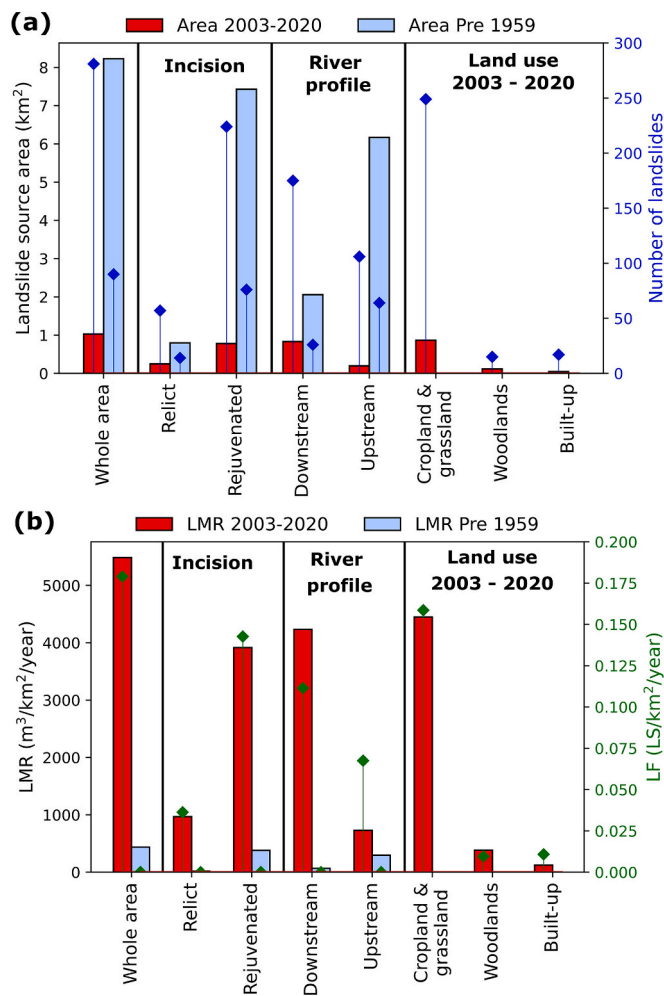
Fig. 11. Landslide source area and number of landslides (a), and landslide frequency and mobilization rates (b) in relation to the rejuvenation by bedrock incision, the position along the river longitudinal profile, and the recent land use. The blue and green diamonds represent the number of landslides and the landslide frequency respectively. LMR: landslide mobilization rate. LF: landslide frequency.

sediment load. However, this does not seem to play an active role in the current incision pattern of the channel; one reason being certainly the limited amount of sediment versus the river discharge.

5.2.4. Step 4: landslides in the Anthropocene

In a landscape, landslides are usually seen as constrains that can potentially have disastrous consequences the population living in their vicinity. But the presence of large stable landslides in the gorge can also here be seen as an opportunity, e.g., by facilitating the creation of hydropower plants. The spread of built-up areas over such large landslides could yet potentially alter their stability conditions. This has been observed in Bukavu where disturbances of the natural slope hydrology and surface and sub-surface runoff water rerouting have led to local increases in pore water pressure and subsequently to an increase in landslide surface displacement (Dille et al., 2022; Mugaruka Bibentyo et al., 2017).

Overall, the study area was already deforested in the 1950's. In the region, the study by Depicker et al. (2021a) shows that, similarly to what is observed in many other regions in the world, deforestation leads to a temporal increase in shallow landslides mobilization rate that lasts 10 to 15 years. Therefore, deforestation that took place >70 years ago cannot be considered to explain the current patterns of shallow landslides. However, these shallow landslides are favoured by the presence of

cropland and grassland, although, as explained in Step 3, topography and lithology remain their main control. As there are very few roads outside the built-up areas in the study area, their potential role on increasing landslide activity cannot be stressed either (Maki Mateso et al., 2023). In the built-up areas, the presence of landslides on slopes less steep than in cropland and grassland areas (Fig. 8) could be the consequence of slope cutting and changes of the surface and subsurface hydrology (Bozzolan et al., 2020; Dille et al., 2022).

The frequency density distribution of the landslides that occurred during the 2003–2020 period (Fig. 7d) indicates that the number of smaller landslides is lower than what could be expected, thereby agreeing with Van Den Eeckhaut et al. (2007) that attribute this underrepresentation to the disappearance of the smallest landslides due to human activities. However, for a rural environment located a few dozen kilometres north, Maki Mateso et al. (2023) did not notice such a human influence. Our study area has quite a limited geographical extent, as compared to that of Maki Mateso et al. (2023) and what we observe here could be local, site-specific characteristics that does not allow us to draw clear conclusions. Nevertheless, we cannot ignore that farming activities and land reclamation in the region favour the disappearance of landslide scars, a process that is further exacerbated by the rapid natural growth of the vegetation. Therefore, we show that the human activities that favour the occurrence of new landslides contributes also to their disappearance from the landscape. Somehow, the current LMRs observed for the recent landslides should not be too far from what we would observe in natural conditions.

5.3. Landslide mobilization rates and non-extreme events

The higher LMRs associated with the small recent landslides (Fig. 11) show another case where high-frequency processes are more important than extreme events associated with the occurrence of large landslides (Roda-Boluda et al., 2018). This trend is even more pronounced when we acknowledge that during our period of observation, the study area was not impacted by highly localised intense convective rainfall that can trigger clusters of hundreds of shallow landslides over limited spatial extent of a few km^2; such clustered landslide events being quite common in the region (Deijns et al., 2022; Maki Mateso et al., 2023). The LMRs associated with small shallow landslides are higher than those found by Broeckx et al. (2019) in the Mount Elgon region in Uganda, a somewhat comparable tropical setting in terms of climate and topographic conditions. However, while Mount Elgon is composed of highly weathered rocks of volcanic origin, in our study area, the shallow landslides are mostly controlled by the presence of the metasedimentary rocks, which reveals the key role of lithology at modulating the sediment supply from shallow landslides (Roda-Boluda et al., 2018).

This dominant role of the high-frequency landslides contradicts evidence about the dominant role of large, but rare landslides on LMR (Marc et al., 2019). We could postulate that this is another evidence of the uncommon characteristics of this gorge formation; the exceptional rate of incision having triggered oversized landslides with respect to the local relief, lithological and potential landslide travel distance conditions (Iverson et al., 2015; Korup et al., 2007). The power law relation of the frequency density distribution of the old (pre-1959) landslides (Fig. 7d) indicates a greater role of large, infrequent landslides to the mobilized material (Van Den Eeckhaut et al., 2007). According to the analysis of Malamud et al. (2004), this distribution of historical landslides suggests an unrealistic figure of 10,000 landslides that would have occurred in our study area. Although we know that landslides may increase in size over time (Tanyaş et al., 2018), the size characteristics of the large landslides we have inventoried further evidence the uncommon channel-hillslope coupling in this gorge.

6. Conclusions

We present an analysis of the characteristics and the spatio-temporal
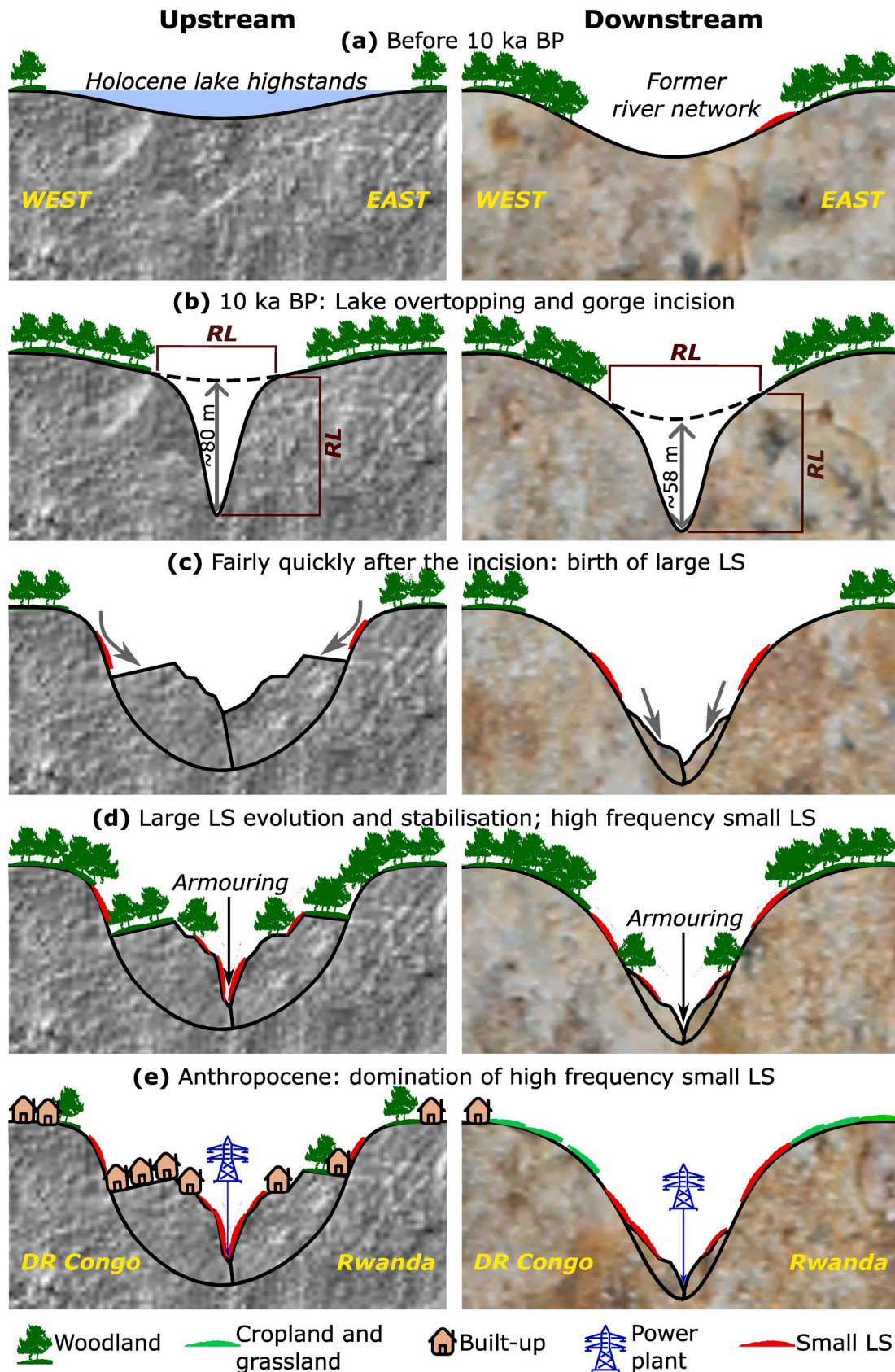
Fig. 12. Conceptual model of the origin and evolution of the landsides in relation to the formation of the Ruzizi Gorge. A differentiation between cross sections of the upstream reach (left) and the downstream reach (right) is made. The grey arrows indicate large landslides. RL: rejuvenated landscape. LS: landslides.

distribution of landslides in the Ruzizi Gorge. We show that the Ruzizi Gorge, formed ~10 ka years ago after the rerouting of the Lake Kivu outflow, represents an exceptional geomorphological landscape of channel formation–hillslope interactions and dynamic feedbacks, where the extremely high incision rates dominated on the lithology for the occurrence of large old landslides. We further demonstrate that these large landslides occurred relatively soon after the incision of the gorge and subsequently, through armouring the river bedrock, contributed to its stabilisation.

The high concentration of large landslides in the gorge makes this section of the Ruzizi River a special regional landslide hotspot. Nevertheless, the LMR associated with the occurrence of this cluster of large landslides is much lower than the LMR associated with the high-frequency smaller landslides. In this specific context of bedrock river incision, the contribution of the extreme landslide event soon after the initiation of the gorge is somehow limited.

The threshold hillslopes associated with the landscape rejuvenation due to the incision of the gorge and the lithological characteristics have more control over the recent shallow landslides than human activities. In addition, the legacy of old landslides, that show very limited to no sign of ongoing deformation, favour also the occurrence of new shallow slope failures. Even under natural vegetation conditions, landslides will likely continue to occur in the study area. Besides the geomorphological context, this study provides useful information for the assessment and potential prevention of landslide hazards in a changing tropical environment.

CRediT authorship contribution statement

Toussaint Mugaruka Bibentyo: Conceptualization, Data curation, Formal analysis, Investigation, Methodology, Resources, Software, Validation, Visualization, Writing – original draft, Writing – review & editing. **Antoine Dille:** Data curation, Formal analysis, Software, Writing – review & editing, Visualization. **Arthur Depicker:** Data curation, Formal analysis, Software, Writing – review & editing. **Benoît Smets:** Data curation, Formal analysis, Software, Writing – review & editing. **Matthias Vanmaercke:** Conceptualization, Supervision, Writing – review & editing. **Charles Nzolang:** Conceptualization, Funding acquisition, Project administration, Supervision, Writing – review & editing. **Stijn Dewaele:** Conceptualization, Supervision, Writing – review & editing. **Olivier Dewitte:** Conceptualization, Funding acquisition, Investigation, Methodology, Project administration, Resources, Supervision, Validation, Writing – review & editing, Data curation, Writing – original draft.

Declaration of competing interest

The authors declare that they have no known competing financial interests or personal relationships that could have appeared to influence the work reported in this paper.

Data availability

Data will be made available on request.

Acknowledgements

Appendix A. Supplementary data

Supplementary data to this article can be found online at https://doi.org/10.1016/j.geomorph.2023.109046.

References

Agatova, A.R., Nepop, R.K., Carling, P.A., Bohorquez, P., Khazin, L.B., Zhdanova, A.N., Moska, P., 2020. Last ice-dammed lake in the Kuray basin, Russian Altai: new results from multidisciplinary research. Earth Sci. Rev. 205, 103183 https://doi.org/10.1016/j.earscirev.2020.103183.

Albino, F., Smets, B., d'Oreye, N., Kervyn, F., 2015. High-resolution TanDEM-X DEM: an accurate method to estimate lava flow volumes at Nyamulagira Volcano (D. R. Congo). J. Geophys. Res. Solid Earth 120, 4189–4207. https://doi.org/10.1002/2015JB011988.

Anton, L., Mather, A.E., Stokes, M., Muñoz-Martin, A., De Vicente, G., 2015. Exceptional river gorge formation from unexceptional floods. Nat. Commun. 6, 7963. https://doi.org/10.1038/ncomms8963.

Azañón, J.M., Azor, A., Pérez-Peña, J.V., Carrillo, J.M., 2005. Late Quaternary large-scale rotational slides induced by river incision: the Arroyo de Gor area (Guadix basin, SE Spain). Geomorphology 69, 152–168. https://doi.org/10.1016/j.geomorph.2004.12.007.

Baynes, E.R.C., Attal, M., Niedermann, S., Kirstein, L.A., Dugmore, A.J., Naylor, M., 2015. Erosion during extreme flood events dominates holocene canyon evolution in northeast Iceland. Proc. Natl. Acad. Sci. U. S. A. 112, 2355–2360. https://doi.org/10.1073/pnas.1415443112.

Bennett, G.L., Miller, S.R., Roering, J.J., Schmidt, D.A., 2016. Landslides, threshold slopes, and the survival of relict terrain in the wake of the Mendocino Triple Junction. Geology 44, 363–366. https://doi.org/10.1130/G37530.1.

Booth, A.M., LaHusen, S.R., Duvall, A.R., Montgomery, D.R., 2017. Holocene history of deep-seated landsliding in the North Fork Stillaguamish River valley from surface roughness analysis, radiocarbon dating, and numerical landscape evolution modeling. J. Geophys. Res. 122, 456–472. https://doi.org/10.1002/2016JF003934.

Bozzolan, E., Holcombe, E., Pianosi, F., Wagener, T., 2020. Including informal housing in slope stability analysis - an application to a data-scarce location in the humid tropics. Nat. Hazards Earth Syst. Sci. 20, 3161–3177. https://doi.org/10.5194/nhess-20-3161-2020.

Broeckx, J., Vanmaercke, M., Duchateau, R., Poesen, J., 2018. A data-based landslide susceptibility map of Africa. Earth Sci. Rev. 185, 102–121. https://doi.org/10.1016/J.EARSCIREV.2018.05.002.

Broeckx, J., Maertens, M., Isabirye, M., Vanmaercke, M., Namazzi, B., Deckers, J., Tamale, J., Jacobs, L., Thiery, W., Kervyn, M., Vranken, L., Poesen, J., 2019. Landslide susceptibility and mobilization rates in the Mount Elgon region, Uganda. Landslides 16, 571–584. https://doi.org/10.1007/s10346-018-1085-y.

Broeckx, J., Rossi, M., Lijnen, K., Campforts, B., Poesen, J., Vanmaercke, M., 2020. Landslide mobilization rates: a global analysis and model. Earth Sci. Rev. 201, 102972 https://doi.org/10.1016/j.earscirev.2019.102972.

Broothaerts, N., Kissi, E., Poesen, J., Van Rompaey, A., Getahun, K., Van Ranst, E., Diels, J., 2012. Spatial patterns, causes and consequences of landslides in the Gilgel Gibe catchment, SW Ethiopia. Catena 97, 127–136. https://doi.org/10.1016/j.catena.2012.05.011.

Burbank, D.W., Leland, J., Fielding, E., Anderson, R.S., Brozovic, N., Reid, M.R., Duncan, C., 1996. Bedrock incision, rock uplift and threshold hillslopes in the northwestern Himalayas. Nature 379, 505–510. https://doi.org/10.1038/379505a0.

Campforts, B., Vanacker, V., Herman, F., Vanmaercke, M., Schwanghart, W., Tenorio, G. E., Willems, P., Govers, G., 2020. Parameterization of river incision models requires accounting for environmental heterogeneity: insights from the tropical Andes. Earth Surf. Dyn. 8, 447–470. https://doi.org/10.5194/esurf-8-447-2020.

Cardinali, M., Reichenbach, P., Guzzetti, F., Ardizzone, F., Antonini, G., Galli, M., Cacciano, M., Castellani, M., Salvati, P., 2002. A geomorphological approach to the estimation of landslide hazards and risks in Umbria, Central Italy. Nat. Hazards Earth Syst. Sci. 2, 57–72. https://doi.org/10.5194/nhess-2-57-2002.

Clarke, B.A., Burbank, D.W., 2010. Bedrock fracturing, threshold hillslopes, and limits to the magnitude of bedrock landslides. Earth Planet. Sci. Lett. 297, 577–586. https://doi.org/10.1016/j.epsl.2010.07.011.

Cook, K.L., Dietze, M., 2019. Short communication: a simple workflow for robust low-cost UAV-derived change detection without ground control points. Earth Surf. Dyn. 7, 1009–1017. https://doi.org/10.5194/esurf-7-1009-2019.

Cook, K.L., Turowski, J.M., Hovius, N., 2013. A demonstration of the importance of bedload transport for fluvial bedrock erosion and knickpoint propagation. Earth Surf. Process. Landf. 38, 683–695. https://doi.org/10.1002/esp.3313.

Cooper, A.H., Brown, T.J., Price, S.J., Ford, J.R., Waters, C.N., 2018. Humans are the most significant global geomorphological driving force of the 21st century. Anthropocene Rev. 5, 222–229. https://doi.org/10.1177/2053019618800234.

Croissant, T., Lague, D., Steer, P., Davy, P., 2017. Rapid post-seismic landslide evacuation boosted by dynamic river width. Nat. Geosci. 10, 680–684. https://doi.org/10.1038/ngeo3005.

Crosta, G.B., Frattini, P., Valbuzzi, E., De Blasio, F.V., 2018. Introducing a new inventory of large Martian landslides. Earth Space Sci. 5, 89–119. https://doi.org/10.1002/2017EA000324.

Defries, R.S., Rudel, T., Uriarte, M., Hansen, M., 2010. Deforestation driven by urban population growth and agricultural trade in the twenty-first century. Nat. Geosci. 3, 178–181. https://doi.org/10.1038/ngeo756.

Deijns, A.J., Dewitte, O., Thiery, W., d'Oreye, N., Malet, J.-P., Kervyn, F., 2022. Timing landslide and flash flood events from SAR satellite: a regionally applicable methodology illustrated in African cloud-covered tropical environments. Nat. Hazards Earth Syst. Sci. 22, 3679–3700. https://doi.org/10.5194/nhess-22-3679-2022.

Delvaux, D., Mulumba, J.L., Sebagenzi, M.N.S., Bondo, S.F., Kervyn, F., Havenith, H.B., 2017. Seismic hazard assessment of the Kivu rift segment based on a new seismotectonic zonation model (western branch, East African Rift system). J. African Earth Sci. 134, 831–855. https://doi.org/10.1016/j.jafrearsci.2016.10.004.

Depicker, A., Jacobs, L., Delvaux, D., Havenith, H.-B., Maki Mateso, J.C., Govers, G., Dewitte, O., 2020. The added value of a regional landslide susceptibility assessment: the western branch of the East African Rift. Geomorphology 353, 106886. https://doi.org/10.1016/j.geomorph.2019.106886.

Depicker, A., Govers, G., Jacobs, L., Campforts, B., Uwihirwe, J., Dewitte, O., 2021a. Interactions between deforestation, landscape rejuvenation, and shallow landslides in the North Tanganyika-Kivu rift region, Africa. Earth Surf. Dyn. 9, 445–462. https://doi.org/10.5194/esurf-9-445-2021.

Depicker, A., Jacobs, L., Mboga, N., Smets, B., Van Rompaey, A., Lennert, M., Wolff, E., Kervyn, F., Michellier, C., Dewitte, O., Govers, G., 2021b. Historical dynamics of landslide risk from population and forest-cover changes in the Kivu Rift. Nat. Sustain. 4, 965–974. https://doi.org/10.1038/s41893-021-00757-9.

Dewitte, O., Van Den Eeckhaut, M., Poesen, J., Demoulin, A., 2009. Decadal-scale analysis of ground movements in old landslides in western Belgium. Z. Geomorphol. 53, 23–45. https://doi.org/10.1127/0372-8854/2009/0053-0023.

Dewitte, O., Dille, A., Depicker, A., Kubwimana, D., Maki Mateso, J.-C., Mugaruka Bibentyo, T., Uwihirwe, J., Monsieurs, E., 2021. Constraining landslide timing in a data-scarce context: from recent to very old processes in the tropical environment of the North Tanganyika-Kivu Rift region. Landslides 18, 161–177. https://doi.org/10.1007/s10346-020-01452-0.

Dewitte, O., Depicker, A., Moeyersons, J., Dille, A., 2022. Mass movements in tropical climates. In: Shroder, J.J.F. (Ed.), Treatise on Geomorphology, vol. 5. Elsevier, Academic Press, pp. 338–349. https://doi.org/10.1016/B978-0-12-818234-5.00118-8.

Dille, A., Kervyn, F., Mugaruka Bibentyo, T., Delvaux, D., Bamulezi Ganza, G., Ilombe Mawe, G., Kalikone Buzera, C., Safari Nakito, E., Moeyersons, J., Monsieurs, E., Nzolang, C., Smets, B., Kervyn, M., Dewitte, O., 2019. Causes and triggers of deep-seated hillslope instability in the tropics – insights from a 60-year record of Ikoma landslide (DR Congo). Geomorphology 345, 106835. https://doi.org/10.1016/j.geomorph.2019.106835.

Dille, A., Dewitte, O., Handwerger, A.L., d'Oreye, N., Derauw, D., Bamulezi Ganza, G., Ilombe Mawe, G., Michellier, C., Moeyersons, J., Monsieurs, E., Mugaruka Bibentyo, T., Samsonov, S., Smets, B., Kervyn, M., Kervyn, F., 2022. Acceleration of a large deep-seated tropical landslide due to urbanization feedbacks. Nat. Geosci. 15, 1048–1055. https://doi.org/10.1038/s41561-022-01073-3.

Fan, N., Chu, Z., Jiang, L., Hassan, M.A., Lamb, M.P., Liu, X., 2018. Abrupt drainage basin reorganization following a Pleistocene river capture. Nat. Commun. 9, 3756. https://doi.org/10.1038/s41467-018-06238-6.

Felton, A.A., Russell, J.M., Cohen, A.S., Baker, M.E., Chesley, J.T., Lezzar, K.E., McGlue, M.M., Pigati, J.S., Quade, J., Curt Stager, J., Tiercelin, J.J., 2007. Paleolimnological evidence for the onset and termination of glacial aridity from Lake Tanganyika, Tropical East Africa. Palaeogeogr. Palaeoclimatol. Palaeoecol. 252, 405–423. https://doi.org/10.1016/J.PALAEO.2007.04.003.

Fernandez-Alonso, M., Cutten, H., De Waele, B., Tack, L., Tahon, A., Baudet, D., Barritt, S.D., 2012. The Mesoproterozoic Karagwe-Ankole Belt (formerly the NE Kibara Belt): the result of prolonged extensional intracratonic basin development punctuated by two short-lived far-field compressional events. Precambrian Res. 216–219, 63–86. https://doi.org/10.1016/j.precamres.2012.06.007.

Frattini, P., Crosta, G.B., 2013. The role of material properties and landscape morphology on landslide size distributions. Earth Planet. Sci. Lett. 361, 310–319. https://doi.org/10.1016/j.epsl.2012.10.029.

Guns, M., Vanacker, V., 2014. Shifts in landslide frequency-area distribution after forest conversion in the tropical Andes. Anthropocene 6, 75–85. https://doi.org/10.1016/j.ancene.2014.08.001.

Gupta, S., Collier, J.S., Palmer-Felgate, A., Potter, G., 2007. Catastrophic flooding origin of shelf valley systems in the English Channel. Nature 448, 342–345. https://doi.org/10.1038/nature06018.

Guzzetti, F., Mondini, A.C., Cardinali, M., Fiorucci, F., Santangelo, M., Chang, K.T., 2012. Landslide inventory maps: new tools for an old problem. Earth Sci. Rev. 112, 42–66. https://doi.org/10.1016/j.earscirev.2012.02.001.

Haberyan, K.A., Hecky, R.E., 1987. The late Pleistocene and Holocene stratigraphy and paleolimnology of Lakes Kivu and Tanganyika. Palaeogeogr. Palaeoclimatol. Palaeoecol. 61, 169–197. https://doi.org/10.1016/0031-0182(87)90048-4.

Henriques, C., Zêzere, J.L., Marques, F., 2015. The role of the lithological setting on the landslide pattern and distribution. Eng. Geol. 189, 17–31. https://doi.org/10.1016/j.enggeo.2015.01.025.

Hosmer, D.W., Lemeshow, S., Sturdivant, R.X., 2013. Applied Logistic Regression, 3rd ed. John Wiley & Sons.

Hungr, O., Leroueil, S., Picarelli, L., 2014. The Varnes classification of landslide types, an update. Landslides 11, 167–194. https://doi.org/10.1007/s10346-013-0436-y.

Ilunga, L., 1984. Le quaternaire de la plaine de la Ruzizi (Etude morphologique et lithostratigraphique). Vrije Universiteit Bruxelles, Belgium.

Ilunga, L., 2007. Environnements sédimentaires et minéralogie des formations superficielles de la Plaine de la Ruzizi (Nord du Lac Tanganyika). Geo-Eco-Trop 31, 71–144.

Ilunga, L., Alexandre, J., 1982. La géomorphologie de la plaine de la Ruzizi. Analyse et cartographie. Géo-Eco-Trop. Revue Internationale d'écologie et de Géographie Tropicales, Tervuren, 6, pp. 105–123.

Iverson, R.M., George, D.L., Allstadt, K., Reid, M.E., Collins, B.D., Vallance, J.W., Schilling, S.P., Godt, J.W., Cannon, C.M., Magirl, C.S., Baum, R.L., Coe, J.A., Schulz, W.H., Bower, J.B., 2015. Landslide mobility and hazards: implications of the 2014 Oso disaster. Earth Planet. Sci. Lett. 412, 197–208. https://doi.org/10.1016/j.epsl.2014.12.020.

Jacobs, L., Dewitte, O., Poesen, J., Maes, J., Mertens, K., Sekajugo, J., Kervyn, M., 2017. Landslide characteristics and spatial distribution in the Rwenzori Mountains, Uganda. J. Afr. Earth Sci. 134, 917–930. https://doi.org/10.1016/j.jafrearsci.2016.05.013.

Jacobs, L., Dewitte, O., Poesen, J., Sekajugo, J., Nobile, A., Rossi, M., Thiery, W., Kervyn, M., 2018. Field-based landslide susceptibility assessment in a data-scarce environment: the populated areas of the Rwenzori Mountains. Nat. Hazards Earth Syst. Sci. 18, 105–124. https://doi.org/10.3929/ETHZ-B-000234015.

Kampunzu, A.B., Vellutini, P.J., Caron, J.P., Lubala, R.T., Kanika, M., 1983. Le volcanisme et l'evolution structurale du Sud-Kivu (Zaire). Un modele d'interpretation geodynamique du volcanisme distensif intracontinental. Bull. Centres Rech. Explor. Prod. Elf-Aquitaine 7, 257–271.

Kanika, M., Kampunzu, A.B., Caron, J.P.H., Vellutini, P.J., 1981. Données nouvelles sur le volcanisme de la haute Ruzizi (Sud Kivu, Zaïre). CR Acad. Sci. Paris 292, 1277–1282.

Keaton, J.R., DeGraff, J.V., 1996. Surface observation and geologic mapping. In: Turner, A.K., Schuster, R.L. (Eds.), Landslides: Investigation and Mitigation. Spec. Rep., 247, Transp. Res. Board, Natl. Res. Council, Washington, D. C.

Kirschbaum, D.B., Adler, R., Hong, Y., Kumar, S., Peters-Lidard, C., Lerner-Lam, A., 2012. Advances in landslide nowcasting: Evaluation of a global and regional modeling approach. Environ. Earth Sci. 66, 1683–1696. https://doi.org/10.1007/s12665-011-0990-3.

Korup, O., 2006. Effects of large deep-seated landslides on hillslope morphology, western Southern Alps, New Zealand. J. Geophys. Res 111, F01018. https://doi.org/10.1029/2004JF000242.

Korup, O., Weidinger, J.T., 2011. Rock type, precipitation, and the steepness of Himalayan threshold hillslopes. Geol. Soc. Lond. Spec. Publ. 353, 235–249. https://doi.org/10.1144/SP353.12.

Korup, O., Clague, J.J., Hermanns, R.L., Hewitt, K., Strom, A.L., Weidinger, J.T., 2007. Giant landslides, topography, and erosion. Earth Planet. Sci. Lett. 261, 578–589. https://doi.org/10.1016/j.epsl.2007.07.025.

Kubwimana, D., Brahim, L.A., Nkurunziza, P., Dille, A., Depicker, A., Nahimana, L., Abdelouafi, A., Dewitte, O., 2021. Characteristics and distribution of landslides in the populated Hillslopes of Bujumbura, Burundi. Geosciences 11, 259. https://doi.org/10.3390/geosciences11060259.

Lamb, M.P., Fonstad, M.A., 2010. Rapid formation of a modern bedrock canyon by a single flood event. Nat. Geosci. 3, 477–481. https://doi.org/10.1038/ngeo894.

Lambin, E.F., Geist, H., Rindfuss, R.R., 2006. Introduction: Local Processes with Global Impacts. In: Lambin, E.F., Geist, H. (Eds.), Land-Use and Land-Cover Change. Global Change - the IGBP Series. Springer, Berlin, Heidelberg. https://doi.org/10.1007/3-540-32202-7_1.

Larsen, I.J., Montgomery, D.R., 2012. Landslide erosion coupled to tectonics and river incision. Nat. Geosci. 5, 468–473. https://doi.org/10.1038/ngeo1479.

Larsen, I.J., Montgomery, D.R., Korup, O., 2010. Landslide erosion controlled by hillslope material. Nat. Geosci. 3, 247–251. https://doi.org/10.1038/ngeo776.

Lee, S., Pradhan, B., 2007. Landslide hazard mapping at Selangor, Malaysia using frequency ratio and logistic regression models. Landslides 4, 33–41. https://doi.org/10.1007/s10346-006-0047-y.

Leprince, S., Ayoub, F., Klinger, Y., Avouac, J.P., 2007. Co-Registration of Optically Sensed Images and Correlation (COSI-Corr): An Operational Methodology for Ground Deformation Measurements, 1943–1946. International Geoscience and Remote Sensing Symposium (IGARSS). https://doi.org/10.1109/IGARSS.2007.4423207.

Lewis, S.L., Maslin, M.A., 2015. A transparent framework for defining the Anthropocene Epoch. Anthropocene Rev. 2, 128–146. https://doi.org/10.1177/2053019615588792.

Mackey, B.H., Roering, J.J., 2011. Sediment yield, spatial characteristics, and the long-term evolution of active earthflows determined from airborne LiDAR and historical aerial photographs, Eel River, California. GSA Bull. 123, 1560–1576. https://doi.org/10.1130/B30306.1.

Maki Mateso, J.-C., Bielders, C.L., Monsieurs, E., Depicker, A., Smets, B., Tambala, T., Bagalwa Mateso, L., Dewitte, O., 2023. Characteristics and causes of natural and human-induced landslides in a tropical mountainous region: the rift flank west of

Lake Kivu (Democratic Republic of the Congo). Nat. Hazards Earth Syst. Sci. 23, 643–666. https://doi.org/10.5194/nhess-23-643-2023.

Malamud, B.D., Turcotte, D.L., Guzzetti, F., Reichenbach, P., 2004. Landslide inventories and their statistical properties. Earth Surf. Process. Landf. 29, 687–711. https://doi.org/10.1002/esp.1064.

Marc, O., Behling, R., Andermann, C., Turowski, J.M., Illien, L., Roessner, S., Hovius, N., 2019. Long-term erosion of the Nepal Himalayas by bedrock landsliding: the role of monsoons, earthquakes and giant landslides. Earth Surf. Dyn. 7, 107–128. https://doi.org/10.5194/esurf-7-107-2019.

Mather, A.E., Stokes, M., 2018. Bedrock structural control on catchment-scale connectivity and alluvial fan processes, High Atlas Mountains, Morocco. Geol. Soc. Special Pub. 440, 103–128. https://doi.org/10.1144/SP440.15.

Michellier, C., 2017. Contribuer à la prévention des risques d'origine géologique : l'évaluation de la vulnérabilité des populations dans un contexte de rareté de données. Université Libre de Bruxelles, Les cas de Goma et Bukavu (RD Congo).

Monsieurs, E., Jacobs, L., Michellier, C., Basimike Tchangaboba, J., Bamulezi Ganza, G., Kervyn, F., Maki Mateso, J.-C., Mugaruka Bibentyo, T., Kalikone Buzera, C., Nahimana, L., Ndayisenga, A., Nkurunziza, P., Thiery, W., Demoulin, A., Kervyn, M., Dewitte, O., 2018. Landslide inventory for hazard assessment in a data-poor context: a regional-scale approach in a tropical African environment. Landslides 15, 2195–2209. https://doi.org/10.1007/s10346-018-1008-y.

Mugaruka Bibentyo, T., Kulimushi Matabaro, S., Muhindo, S.W., Dewitte, O., 2017. Anatomy of Nyakavogo landslide (Bukavu, DR Congo): interplay between natural and anthropogenic factors. Geo-Eco-Trop 41, 249–262.

Muvundja, F.A., Wüest, A., Isumbisho, M., Kaningini, M.B., Pasche, N., Rinta, P., Schmid, M., 2014. Modelling lake kivu water level variations over the last seven decades. Limnologica 47, 21–33. https://doi.org/10.1016/j.limno.2014.02.003.

Muvundja, F.A., Walumona, J.R., Dusabe, M.C., Alunga, G.L., Kankonda, A.B., Albrecht, C., Eisenberg, J., Wüest, A., 2022. The land–water–energy nexus of Ruzizi River Dams (Lake Kivu Outflow, African Great Lakes Region): status, challenges, and Perspectives. Front. Environ. Sci. 10, 1–14. https://doi.org/10.3389/fenvs.2022.892591.

Nibigira, L., Havenith, H.-B., Archambeau, P., Dewals, B., 2018. Formation, breaching and flood consequences of a landslide dam near Bujumbura, Burundi. Nat. Hazards Earth Syst. Sci. 18, 1867–1890. https://doi.org/10.5194/nhess-18-1867-2018.

Nobile, A., Dille, A., Monsieurs, E., Basimike, J., Mugaruka Bibentyo, T., d'Oreye, N., Kervyn, F., Dewitte, O., 2018. Multi-temporal DInSAR to characterise landslide ground deformations in a tropical urban environment: focus on Bukavu (DR Congo). Remote Sens. (Basel) 10, 626. https://doi.org/10.3390/rs10040626.

Ouimet, W.B., Whipple, K.X., Royden, L.H., Sun, Z., Chen, Z., 2007. The influence of large landslides on river incision in a transient landscape: Eastern margin of the Tibetan Plateau (Sichuan, China). GSA Bull. 119, 1462–1476. https://doi.org/10.1130/B26136.1.

Pánek, T., Břežný, M., Kapustová, V., Lenart, J., Chalupa, V., 2019. Large landslides and deep-seated gravitational slope deformations in the Czech Flysch Carpathians: new LiDAR-based inventory. Geomorphology 346, 106852. https://doi.org/10.1016/j.geomorph.2019.106852.

Peel, M.C., Finlayson, B.L., McMahon, T.A., 2007. Updated world map of the Köppen-Geiger climate classification. Hydrol. Earth Syst. Sci. 11, 1633–1644. https://doi.org/10.5194/hess-11-1633-2007.

Reichenbach, P., Rossi, M., Malamud, B.D., Mihir, M., Guzzetti, F., 2018. A review of statistically-based landslide susceptibility models. Earth Sci. Rev. 180, 60–91. https://doi.org/10.1016/j.earscirev.2018.03.001.

Roda-Boluda, D.C., D'Arcy, M., McDonald, J., Whittaker, A.C., 2018. Lithological controls on hillslope sediment supply: insights from landslide activity and grain size

distributions. Earth Surf. Process. Landf. 43, 956–977. https://doi.org/10.1002/esp.4281.

Ross, K.A., Smets, B., De Batist, M., Hilbe, M., Schmid, M., Anselmetti, F.S., 2014. Lake-level rise in the late Pleistocene and active subaquatic volcanism since the Holocene in Lake Kivu, East African Rift. Geomorphology 221, 274–285. https://doi.org/10.1016/j.geomorph.2014.05.010.

Rupnik, E., Daakir, M., Pierrot Deseilligny, M., 2017. MicMac – a free, open-source solution for photogrammetry. Open Geospatial Data, Softw. Stand. 2, 14. https://doi.org/10.1186/s40965-017-0027-2.

Samia, J., Temme, A., Bregt, A., Wallinga, J., Guzzetti, F., Ardizzone, F., Rossi, M., 2017. Do landslides follow landslides? Insights in path dependency from a multi-temporal landslide inventory. Landslides 14, 547–558. https://doi.org/10.1007/s10346-016-0739-x.

Samsonov, S., Dille, A., Dewitte, O., Kervyn, F., d'Oreye, N., 2020. Satellite interferometry for mapping surface deformation time series in one, two and three dimensions: a new method illustrated on a slow-moving landslide. Eng. Geol. 266, 105471 https://doi.org/10.1016/j.enggeo.2019.105471.

Schanz, S.A., Montgomery, D.R., 2016. Lithologic controls on valley width and strath terrace formation. Geomorphology 258, 58–68. https://doi.org/10.1016/j.geomorph.2016.01.015.

Shobe, C.M., Turowski, J.M., Nativ, R., Glade, R.C., Bennett, G.L., Dini, B., 2021. The role of infrequently mobile boulders in modulating landscape evolution and geomorphic hazards. Earth Sci. Rev. 220, 103717 https://doi.org/10.1016/j.earscirev.2021.103717.

Sidle, R., Ochiai, H., 2006. Landslides: processes, prediction, and land use. In: American Geophysical Union, Water Resources Monograph, Washington, USA. https://doi.org/10.1029/WM018.

Stoffers, P., Hecky, R. E., 1978. Late Pleistocene–; Holocene Evolution of the Kivu–Tanganyika Basin. Mod. Anc. Lake Sediments 2, 43–55. doi:https://doi.org/10.1002/9781444303698.ch3.

Tanyaş, H., Allstadt, K.E., van Westen, C.J., 2018. An updated method for estimating landslide-event magnitude. Earth Surf. Process. Landf. 43, 1836–1847. https://doi.org/10.1002/esp.4359.

Van Den Eeckhaut, M., Poesen, J., Govers, G., Verstraeten, G., Demoulin, A., 2007. Characteristics of the size distribution of recent and historical landslides in a populated hilly region. Earth Planet. Sci. Lett. 256, 588–603. https://doi.org/10.1016/j.epsl.2007.01.040.

Villeneuve, M., 1977. Precambrien du sud du lac Kivu (Region du Kivu, République du zaïre). Etude stratigraphique, pétrographique et téctonique. Université d'Aix-Marseille III.

Villeneuve, M., Chorowicz, J., 2004. Les sillons plissés du Burundien supérieur dans la châne Kibarienne d'Afrique centrale. Comptes Rendus - Geoscience 336, 807–814. https://doi.org/10.1016/j.crte.2004.01.006.

Whipple, K.X., DiBiase, R.A., Crosby, B., Johnson J.P.L., 2022. 6.40 - Bedrock Rivers, in: Shroder, J.J.F. (Eds.), Treatise on Geomorphology (Second Edition). Academic Press, pp. 865–903. doi:https://doi.org/10.1016/B978-0-12-818234-5.00101-2.

Williams, F., McColl, S., Fuller, I., Massey, C., Smith, H., Neverman, A., 2021. Intersection of fluvial incision and weak geologic structures cause divergence from a universal threshold slope model of landslide occurrence. Geomorphology 389, 107795. https://doi.org/10.1016/j.geomorph.2021.107795.

Yenes, M., Monterrubio, S., Nespereira, J., Santos, G., Fernández-Macarro, B., 2015. Large landslides induced by fluvial incision in the Cenozoic Duero Basin (Spain). Geomorphology 246, 263–276. https://doi.org/10.1016/j.geomorph.2015.06.022.